



Natural Resources
Canada

Ressources naturelles
Canada

**GEOLOGICAL SURVEY OF CANADA
OPEN FILE 8185**

**Sediment response investigations in Kitimat,
British Columbia: geophysical data sets**

**A.J-M. Pugin, B. Dietiker, H. Crow, K. Brewer, C. Brillon,
T. Cartwright, J.F. Cassidy, and J.A. Hunter**

2018

Canada 



GEOLOGICAL SURVEY OF CANADA OPEN FILE 8185

Sediment response investigations in Kitimat, British Columbia: geophysical data sets

**A. J-M. Pugin, B. Dietiker, H. Crow, K. Brewer, C. Brillon, T. Cartwright,
J.F. Cassidy, and J.A. Hunter**

2018

© Her Majesty the Queen in Right of Canada, as represented by the Minister of Natural Resources, 2018

Information contained in this publication or product may be reproduced, in part or in whole, and by any means, for personal or public non-commercial purposes, without charge or further permission, unless otherwise specified.

You are asked to:

- exercise due diligence in ensuring the accuracy of the materials reproduced;
- indicate the complete title of the materials reproduced, and the name of the author organization; and
- indicate that the reproduction is a copy of an official work that is published by Natural Resources Canada (NRCan) and that the reproduction has not been produced in affiliation with, or with the endorsement of, NRCan.

Commercial reproduction and distribution is prohibited except with written permission from NRCan. For more information, contact NRCan at nrcan.copyrightdroitdauteur.nrcan@canada.ca.

Permanent link: <https://doi.org/10.4095/300556>

This publication is available for free download through GEOSCAN (<http://geoscan.nrcan.gc.ca/>).

Recommended citation

Pugin, A.J.-M., Dietiker, B., Crow, H., Brewer, K., Brillon, C., Cartwright, T., Cassidy, J.F., and Hunter, J.A., 2018. Sediment response investigations in Kitimat, British Columbia: geophysical data sets; Geological Survey of Canada, Open File 8185, 1 .zip file. <https://doi.org/10.4095/300556>

Contents

1.0	Introduction.....	3
2.0	Geophysical Survey Methods	10
3.0	Results and Interpretation	23
4.0	Conclusions.....	36
5.0	Acknowledgements	37
6.0	References.....	38

1.0 Introduction

The Geological Survey of Canada (GSC) leads research across Canada on natural hazards which have the potential to negatively impact communities, critical infrastructure, and the environment. Since 2013, the GSC has undertaken a range of activities to improve the assessment of geohazards (specifically earthquakes, tsunamis, and landslides) in British Columbia's North Coast (BCNC) region as part of the World-Class Tanker Safety Initiative. This initiative includes targeted mapping, monitoring, and modelling of selected marine and terrestrial coastal geohazards in and around the district of Kitimat, BC (e.g. Brillon, 2016; Shaw et al., 2017; Conway and Barrie 2018; Stacey et al., 2018). The terrestrial aspect of this work has included the installation of two new broadband seismograph stations at reference bedrock and soil sites in Kitimat, and numerous seismograph and GPS monitoring stations in the surrounding BCNC region.

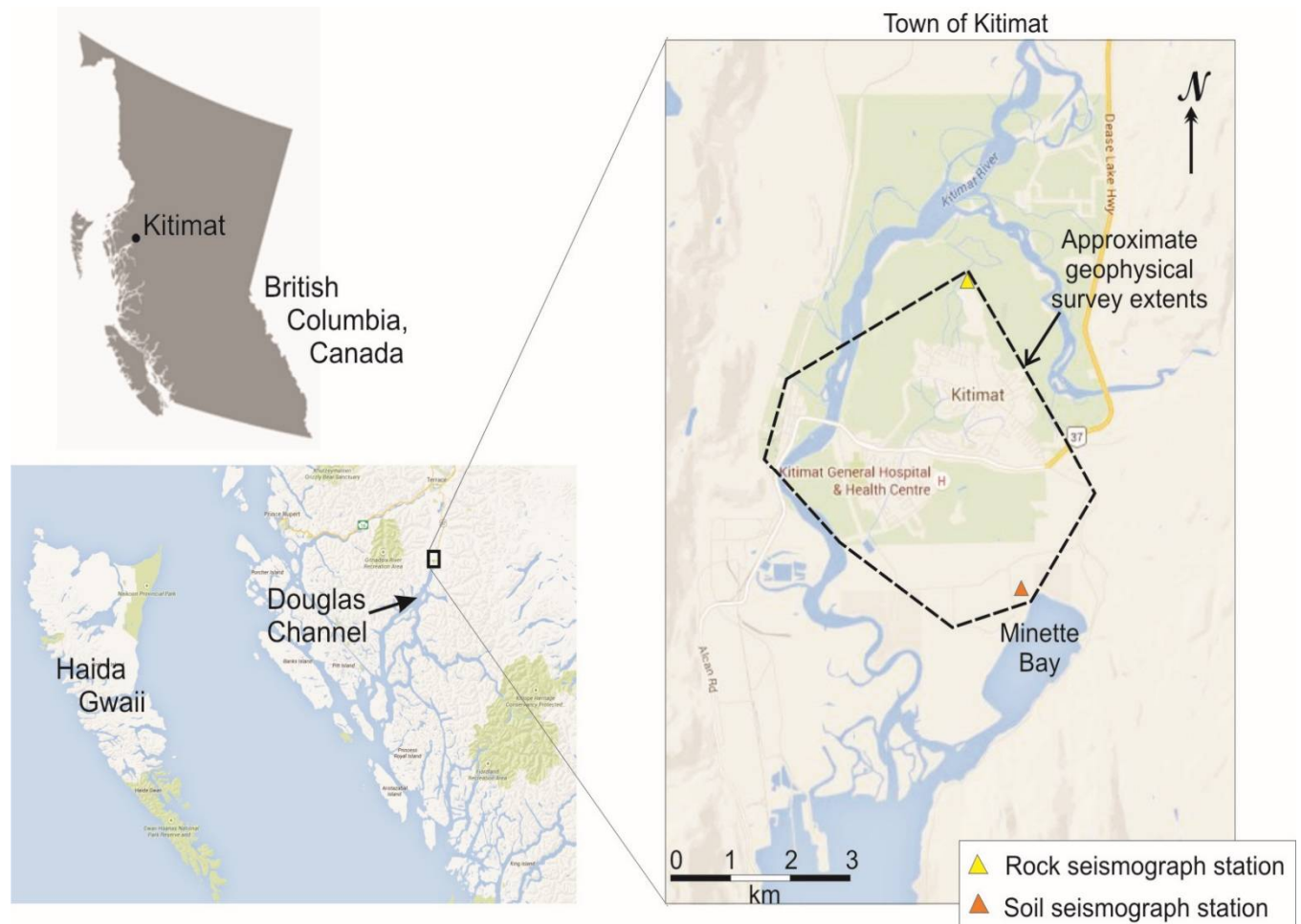


Figure 1 - Map of Kitimat with locations of soil and rock seismic stations in town.

In support of the terrestrial work, the GSC is carrying out seismic surveys on public lands within the town of Kitimat (Figure 1). It is well recognised that unconsolidated materials over bedrock can amplify earthquake energy at surface (Anderson et al., 1986; Martin and Dobry, 1994; Anderson et al., 1996; Kramer, 1996). This effect can be greatly increased when the impedance contrast between soil and bedrock stiffness is large (i.e. Hunter et al., 2010).

To better predict earthquake-induced ground motions in Kitimat, a three-phased study of the unconsolidated sediments filling the Kitimat Valley was initiated in 2014. In the first phase of the investigation, 27 Horizontal-to-Vertical Spectral Ratio (HVSr) measurements were collected in the town of Kitimat to assess the variation in fundamental site frequencies within the valley (Brillon et al., 2015) which are influenced by the thickness of the sediment column overlying the main seismic impedance contrast (often bedrock or dense till). The following year, an additional 53 HVSr recordings were collected (Crow et al., 2015a). These results were analysed to guide the selection of high-resolution seismic reflection profile alignments collected during the second phase of the investigation, undertaken in June of 2015. The basin structure and sediment velocity information interpreted from 14 line-km of seismic profiles will provide needed information for a third phase of the investigation comprised of ground motion modelling scenarios. A downhole seismic log and inverted array measurements were also collected and interpreted during the second phase of the investigation. An improved understanding of local earthquake site response in this area of significant new infrastructure development may directly contribute to reduced losses from future large earthquakes.

This report contains the geophysical data collected as part of Phase 1 and Phase 2 of the Kitimat site response study. The report also contains recordings from a M_w 4.6 earthquake which occurred 275 km offshore while seismographs on soil and rock were recording in March of 2014.

1.1 Survey goals and site coverage

The goal of the Kitimat geophysical surveys was to investigate the thickness, structure, and shear wave velocity of unconsolidated sediments overlying bedrock to provide needed information for ground motion response analyses. Geophysical survey coverage presented in this report includes 80 microtremor recordings, 14 line-km of high-resolution seismic reflection profiling, and downhole geophysical logs from one municipal borehole. In addition, publicly available water well logs and seismic cone penetrometer data were reviewed in areas within and around the survey extents (see Section 1.2). Figure 2 presents the various geophysical survey locations along with other publicly available data. Clague's GSC-published 1977 surficial geology map of the region was consulted to help guide the initial selection of locations and alignments for the various geophysical surveys (see Section 1.3).

1.2 Supporting External Datasets

Additional publicly-available borehole datasets were accessed as part of this study, including the BC water well database, on-line Environmental Assessment and National Energy Board reports, and municipal geotechnical reports commissioned by the District of Kitimat. Locations of these borings are shown in Figure 2 and included in a Google Earth file in Appendix A. The information in these borehole datasets was used to assist in the interpretation of the seismic reflection profiles.

Water well data

The online BC water well database (<https://a100.gov.bc.ca/pub/wells/public/indexreports.jsp>) is maintained through the provincial Ministry of the Environment of British Columbia. Data is provided in the form of PDF files containing driller log information which describe lithology in a "from – to" format. Descriptions of the material types are not uniform from well to well; consequently the information was primarily used for checking depth to bedrock (if encountered) and major changes in lithological type. The information was of limited use for the geophysical surveys as very few wells were located on seismic lines (listed in Table 1), and none were open for geophysical logging.

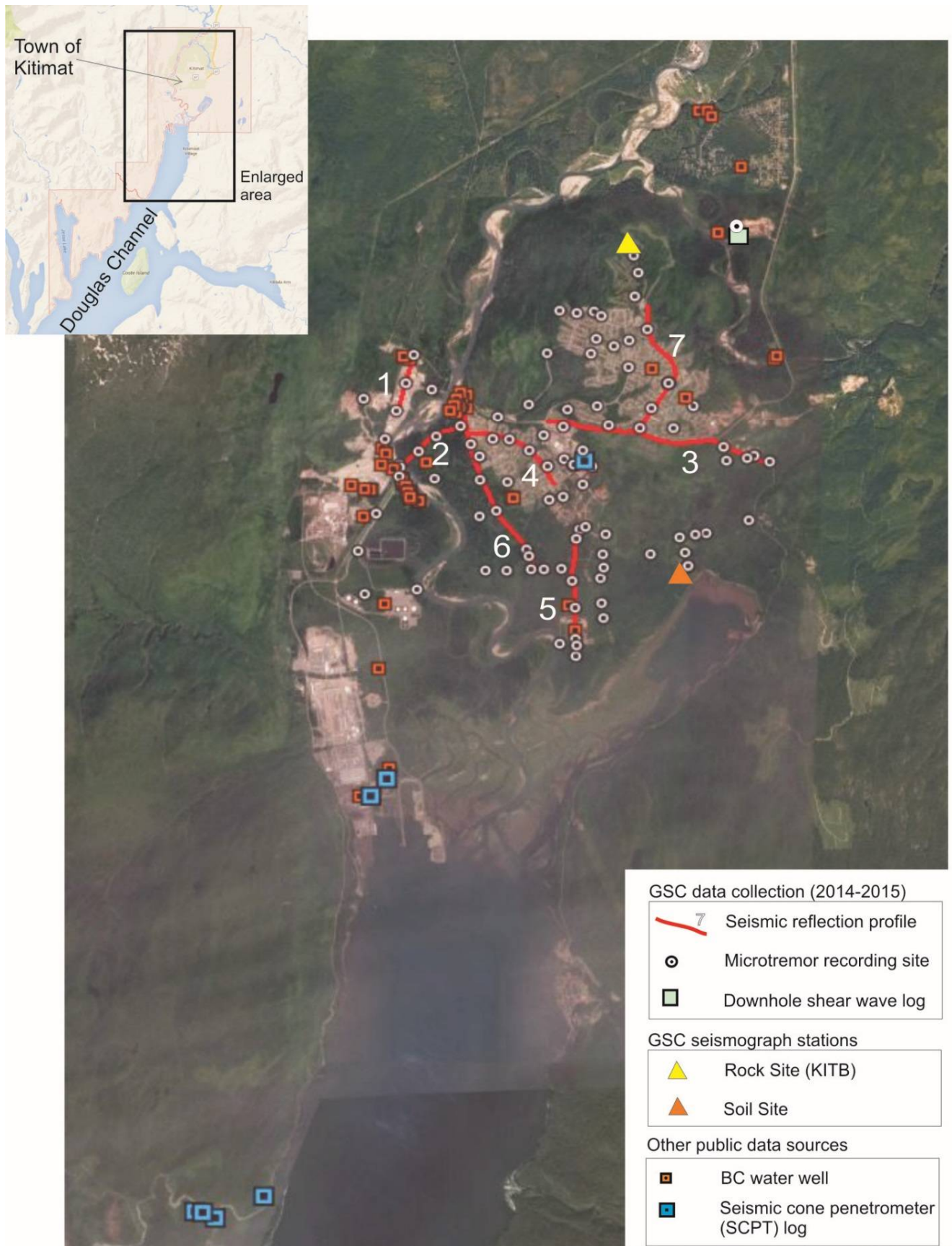


Figure 2 - Geophysical survey data collected by GSC, along with additional sources of publicly available information (BC Water Wells and velocity logs from environmental assessment reports.)

Table 1. Water well records within 100m of seismic lines. Bold records are provided in Appendix E.

Well	x	y	Depth (m)	seismic line		comment
14083	520544.00	5990674.03	9	Line 1	cmp 416	
85378	522997.01	5986451.99	18	Line 5	cmp 714	
107468	522896.02	5986844.02	31	Line 5	cmp 582	
13675	521259.03	5989950.04	18	Line 6	cmp 1269	bedrock at 18 m
13676	521362.00	5989935.05	9	Line 6	cmp 1249	sparse info - not shown
14092	521185.01	5989974.95	7	Line 6	cmp 1281	sparse info - not shown
14095	521212.00	5989857.03	8	Line 6	cmp 1239	sparse info - not shown

External shear wave velocity (Vs) data

Shear wave velocity (Vs) data collected by pushing instrumented seismic cones into the softer marine sediments (silts, sands) around the delta front were used to verify velocities for calibration of seismic profiles. The District of Kitimat had commissioned several past geotechnical studies for municipal development projects in town which were made available to the GSC. For the Kitimat Hospital, a seismic cone penetrometer (SCPT) log (CPT97-06) was carried out at 1 m intervals to measure shear wave velocities to a depth of 45 m (AGRA, 1997). Results are presented on Figure 3.

As part of the government regulatory process for the development of major infrastructure in BC, results from geotechnical studies for Enbridge's Northern Gateway Project (for the National Energy Board) and Rio Tinto Alcan's Terminal A Extension Project (for the BC Government MOE Environmental Assessment) are available online. In a report for Rio Tinto Alcan at their Dredgeate Disposal Site (Golder, 2014), two SCPT logs (SCPT14-4001, SCPT14-4002) were collected to depths of 30 m at the delta front (see Figure 3). These Vs data, presented only as figures in the report, were digitized by the GSC. In a report for Enbridge, four SCPT logs (SCPT06-03, -04, -08, -10) were collected in July 2006 approximately 5 km south of Kitimat to depths ranging between 11 and 24 m. Vs data are presented in tables in a report by AMEC (2010). SCPT data from all seven SCPT borings in marine and glaciomarine sediments (silts, clays, sands) are displayed in Figure 3a. By way of comparison, the velocities are plotted alongside shear wave velocities measured in deep boreholes in the fine grained Fraser River Delta sediments (Hunter et al. (1998), Figure 3b). Results indicate that in both cases, Vs increases with depth and that the lower velocity bound is well constrained. Where intervals of coarser grained materials are present in the deltaic sediments of the Kitimat delta, velocities tend to be higher.

1.3 Geological Setting

The town of Kitimat is located on the farthest inland reach of the Douglas Channel, one of the largest fjords of the BC coast (see Figure 1, Figure 3). From Kitimat, the inland expression of the fjord, the Kitsumkalum-Lakelse Valley, extends some 90 km northward, well beyond the city of Terrace, BC (Dolmage, 1956). It is characterized by steep walls and a relatively flat bottom, up through which smooth rock domes are exposed. Deep drill holes in Terrace and Kitimat (70 and 90 m below sea level respectively) intersected similar marine sediments, suggesting that these materials are continuous along the valley floor and extend out into the fjord (Dolmage, 1956).

Clague (1985) describes two broad material types deposited in the Kitsumkalum-Kitimat Trough during the late Wisconsinan as: massive, bedded, and laminated muds, and stratified sand and gravel. In the

town of Kitimat, these (glacio) marine silts and clays underlie the surficial floodplain sediments (sand and fluvial outwash) of the Kitimat River, and the alluvial fan sediments in tributaries of the Kitimat River north of town (Clague, 1977, compare Figure 4). Borings in the Kitimat area drilled over the past 50 years indicate that the town is underlain by glacial and inter-glacial deposits of gravel, sand, and (glacio) marine clays and silts, up to ~100 m in thickness in some areas. Examples of surficial deposits seen in town were photographed during the fieldwork in 2015 and are presented in Figure 5).

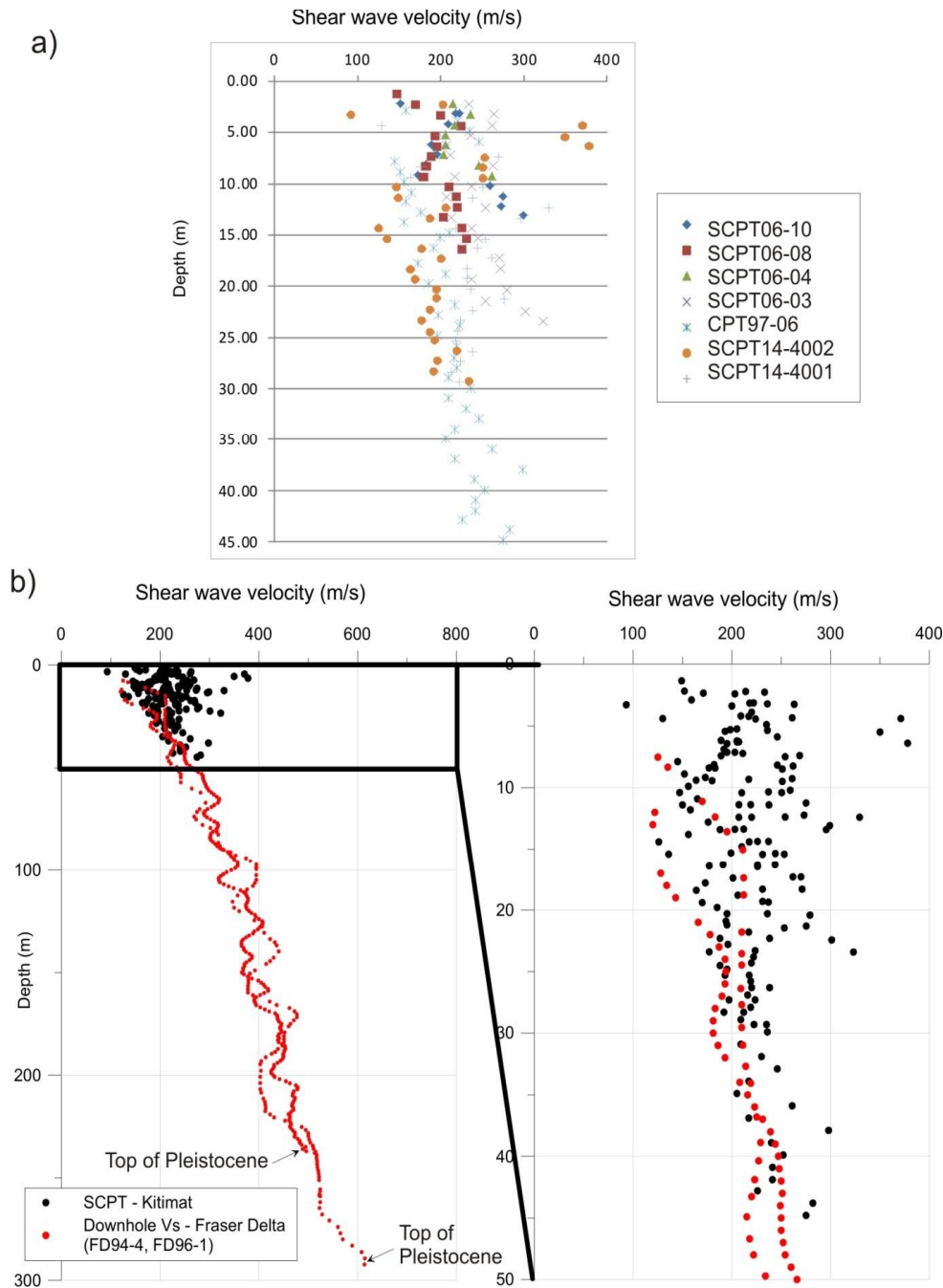


Figure 3 - a) Compilation of publicly available shear wave velocity (Vs) data in fine grained sediments of the Kitimat area collected by private companies using a seismic cone penetrometer (SCPT). b) Comparison of SCPT data in the Kitimat delta with downhole Vs collected in similar sediments in the Fraser River Delta (Hunter et al. 2016)

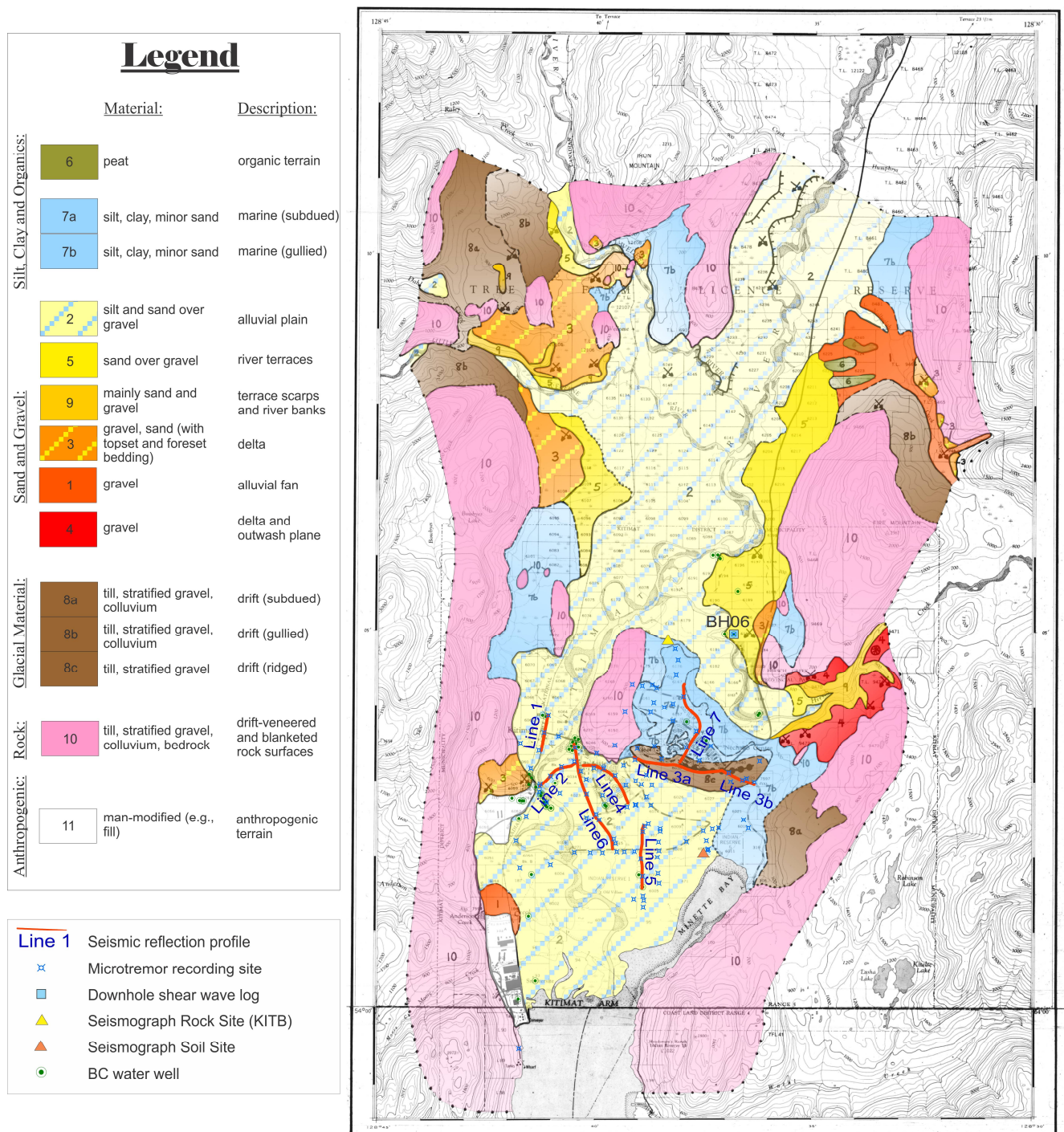


Figure 4 - Surficial geology of the Kitimat area, after Clague (1977) shown with seismic reflection profile alignments.



Figure 5 - Exposures of surficial sediments photographed in Kitimat during 2015 fieldwork. a) marine silt and clay exposed at a residential construction site near seismic line 7; b and c) exposures of sand and gravel on Kitimat river terraces near borehole 06 (surrounding the Kitimat landfill) north of town.

2.0 Geophysical Survey Methods

2.1 Single station microtremor recordings

In areas where soft sediments overlies competent materials (rock or till), energy from vertically traveling weak motion (microtremors) can resonate with very high amplitudes. The frequency, f (or period, $T=1/f$) of this resonance is governed by the average shear wave velocity of the sediment layer overlying the resonating surface, and the thickness of the layer. Nakamura (1989) introduced a method to estimate the fundamental site period, T_0 , or site frequency, f_0 (equivalent to $1/T_0$) using microtremors in the same frequency range as earthquake energy. The horizontal-to-vertical spectral ratio (HVSr) of this recorded noise can indicate a peak frequency equivalent to the resonant frequency of the site. Following on Nakamura's work, between 2001 and 2004, a project named “Site Effects Assessment Using Ambient Excitations” (SESAME) was undertaken by 14 European research institutes which studied the microtremor technique in detail. The guidelines for best practices using this technique have been published (SESAME, 2004) and are now considered standards for the method.

A microseismograph specifically designed for HVSr measurements (a Tromino, manufactured by MoHo s.r.l. in Italy), was used to record microtremor data at 114 sites within the study area. A handheld GPS was used to collect site co-ordinates. Table 2 describes the data collection and processing parameters for the recordings. Processing was carried out using Grilla software, which incorporates the SESAME testing criteria. Of the 114 recordings, 99 were free of excessive noise, and 95 passed all SESAME criteria. The four sites which did not pass failed on only two or three of the six criteria for a clear peak, either because bedrock was near surface (causing a broad, low amplitude peak), or because noise was present in the low frequencies but a clear peak was visible at higher frequencies. Digital files of the resulting frequencies and periods, as well as the acceptance parameters at each test site, are available in Appendix B.

A grid of peak frequencies from all 99 sites was kriged using a linear variogram with a slope of 1 (Figure 6). Peak frequencies ranged between 0.41 – 6.78 Hz with one value reaching 16.31 Hz where bedrock was outcropping nearby as observed during a field visit. Higher frequencies (orange, yellow, green, purple) indicate a resonating layer approaching surface, while lower frequencies (reds) indicate a deeper resonating layer, likely with softer sediment in the near surface. In practice, the vertical and lateral variability of the sediments in the valley, and the topography of the resonating surface(s) make it very difficult to generalize about the subsurface conditions solely using the microtremor method. However, the map does show that the depth to resonator increases to the south approaching the delta, and that deeper valleys (running north-south) cut between outcropping rock domes (purple and dark green). The present-day Kitimat River follows the course of the deep valley to the west.

The recording of an $M_w 4.6$ offshore earthquake in March 2014 (Figure 7) by the microseismograph indicated that the HVSr method is identifying the same resonant frequency whether from microtremor or weak motion earthquake recordings. Therefore, the interpolated fundamental site frequency map (Figure 6) indicates the resonant frequency range most likely to be amplified during an earthquake, and provides a relative sense of whether the resonating surface is shallowing (higher frequencies) or deepening (lower frequencies).

Table 2. Data collection and processing parameters for microtremor measurements.

3-component sampling rate	128 samples/second
Orientation of sensors	approximately N-S, E-W
Recording Time	30 minutes
Processing window	60 seconds
Spectral Filtering	Konno-Omachi Algorithm $b = 40$ (Konno and Omachi, 1998)
Editing	Manual selection of windows with arithmetic averaging
Spectral Windows	0.1 Hz up to 20 Hz (varied by site)

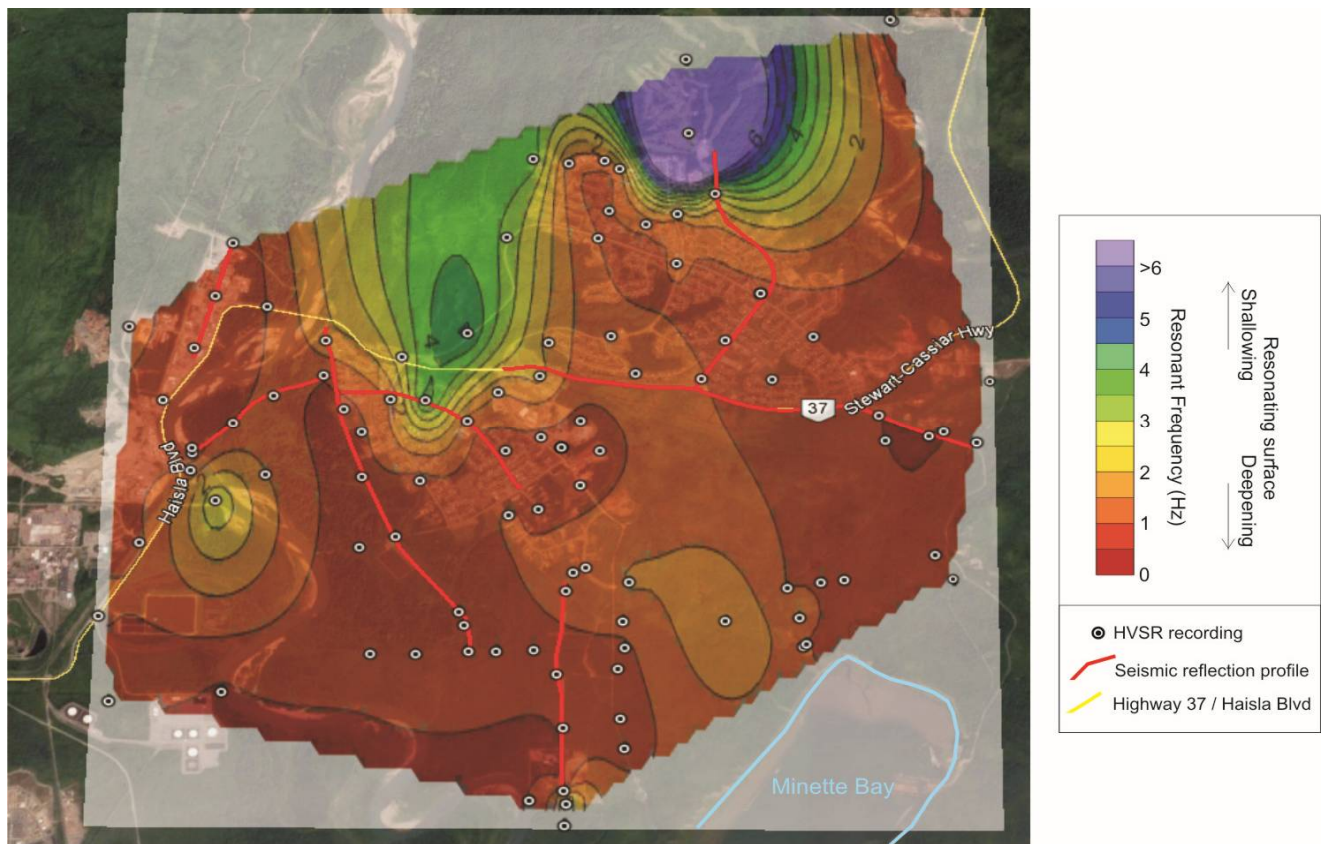


Figure 6 - Contoured resonant frequencies helped guide the selection of seismic reflection profile alignments, shown on map. Deeper resonating surfaces are found in darker red areas (<1 Hz) on the map.

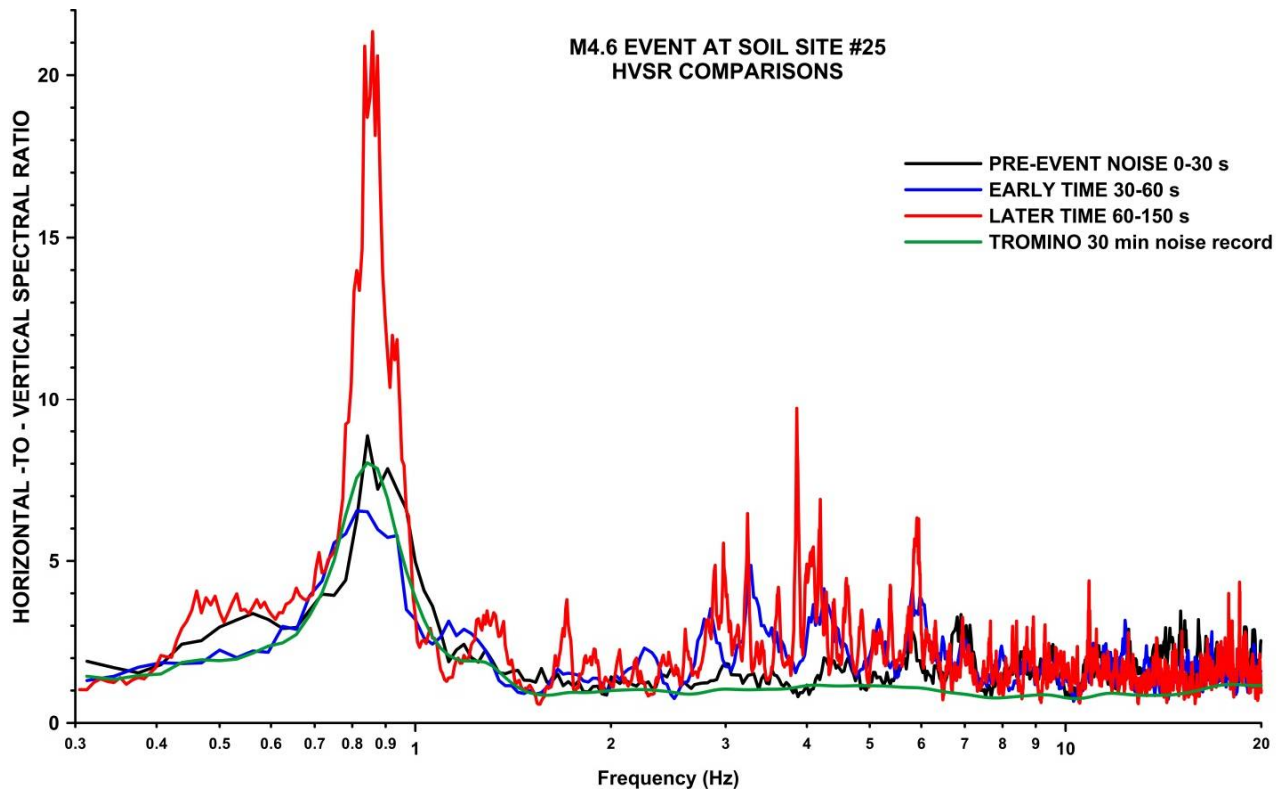


Figure 7 - HVSRs for the M_W 4.6 earthquake event time windows recorded at soil site KIT-25, compared to the 30 minute Tromino ambient noise recording.

2.1.1 Multi-station (array) microtremor recordings

Microtremor data were collected at three sites within the town of Kitimat using an array of five broadband seismographs. An hour of data were recorded for each array configuration, and multiple configurations of increasing station spacings were recorded to achieve a wide dispersion frequency band. Frequency-wavenumber seismic-array processing was applied to estimate surface wave dispersion. The dispersion data were inverted to estimate shear wave velocity and uncertainty, V_{s30} , National Building Code of Canada site classification, and amplification factors. Details of the broadband seismic arrays, processing methods, results, and comparisons with near-by seismic reflection profiles and SCPT data are presented in Gosselin, 2016, Gosselin et al. (2017).

2.2 Borehole geophysical logging

Downhole geophysical logs provide a means of identifying and characterizing lithological units based on variations in their chemical and physical properties. Downhole velocity logs also assist in the conversion of seismic profiles from time to depth sections. A series of municipal PVC-cased monitoring boreholes were available for logging at the Kitimat Landfill, just north of town. As the wells were closely spaced, only the deepest well, BH06, was selected for logging. Although it was not located on a seismic line, the well intersected sand and gravel deposits, which were likely to be encountered on some seismic lines, according to the surficial geology map and BC water well data. Downhole logging techniques included induction methods (magnetic susceptibility) to look for stratigraphic variation in the sand and gravel deposits, and downhole shear wave seismic methods to calculate ranges of V_s in these materials. A more detailed description of the tool theory can be found in Crow et al. (2015b).

Logging was carried out on June 24th, 2015. The magnetic susceptibility log was acquired using a Mount Sopris logging system with a motorized winch and an EM39S susceptibility logging tool manufactured by Geonics Limited. A laptop computer recorded the data using Matrix Logger software. On-site calibrations were carried out pre- and post-run to null the tool. The log was corrected for sensor offsets and casing stick up, and recorded relative to ground surface. The log was run up hole and sampled at 2 cm intervals using an optical encoder connected to the motorized winch.

The shear wave survey was carried out using a downhole 3-component (3-C) wall locking tool with 15 Hz geophones, connected to a Geometrics Geode seismograph. The source consisted of a hammer striking an angled metal plate coupled with the ground, located 1.3 m from the borehole collar. The cable supporting the receiver array was lowered by hand to the bottom of the hole and pulled uphole at 0.5 m spacings, where stationary measurements were made. The data were recorded on a laptop computer after reviewing each record on screen. Records were stacked twice at depths greater than 7.0 m, but only once for depths shallower than 7.0 m. S-wave travel times were picked using a semi-automatic picking program with a pick-to-pick cross-correlation (Ivanov and Miller, 2004). This method selects arrival times through cross-correlation using spline interpolation and requires highly accurate arrival times. Interval velocities were then computed using these interpreted traveltimes plotted against the source-receiver distances. The inverse slope of a three point linear least-squares regression between points provides the layer shear wave velocities between downhole measurement intervals. Additional information on the systems, and field and interpretation procedures developed for downhole S-wave logging are described in greater detail in Hunter and Crow (2015).

Results of the logging are presented in Figure 8, showing results of the two downhole logs collected in BH06 alongside an interpretation of the log response. The stratigraphic description is taken from Gartner Lee (2002) in a report provided to the District of Kitimat. Magnetic susceptibility is more elevated and highly varying in the upper 15 m of the borehole where coarser grained materials (gravel, cobbles, and even boulders) are present. The predominance of gravel is also reflected in the higher shear wave velocities (average $V_s \sim 615$ m/s). The materials encountered in this interval are likely representative of gravel outwash (see 5b, photographed nearby). At depths greater than 15 m, the geophysical logs indicate a decrease in magnetic susceptibility and velocity, which correlates with an overall decrease in grain size (sand, silt, and even some clay) and velocity (average $V_s \sim 270$ m/s). This interval is likely representative of an alluvial sand and silt interval (see Figure 5c, photographed nearby).

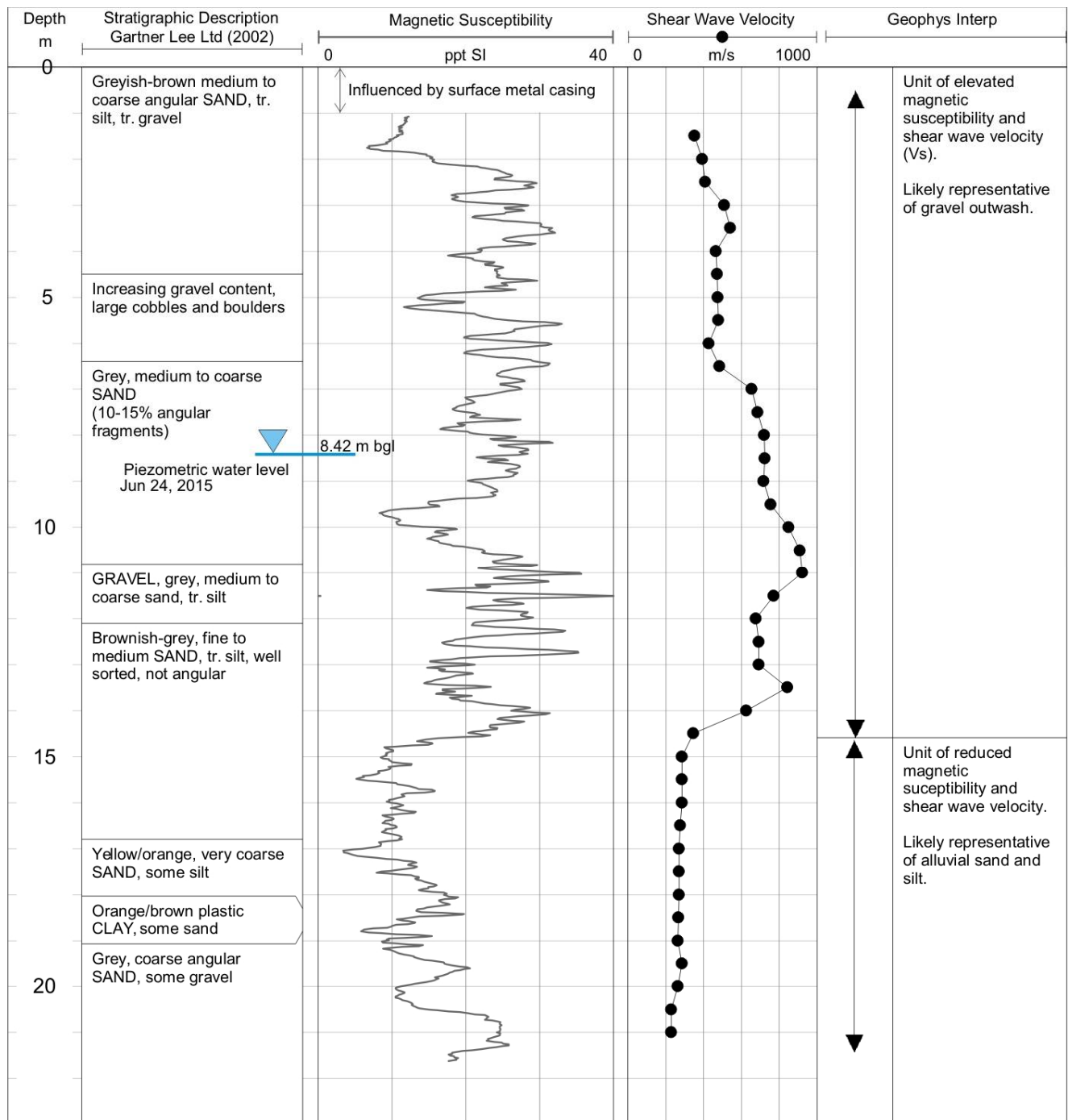


Figure 8 - Downhole geophysical logs from borehole 06 near the Kitimat Landfill site. The borehole is interpreted as intersecting gravel outwash overlying alluvial sand and silt units. Stratigraphic descriptions taken from Gartner Lee (2002) report. “m bgl” = metres below ground level.

2.3 Landstreamer Seismic Surveys

The seismic reflection surveys used a multi-frequency active seismic source (Minivib 1 from Industrial Vehicles International Inc.) towing an array of geophones (a landstreamer). The interpreted profiles provide compressional (P) and shear (S) wave velocities, along with information on sediment stratigraphy and depth to resonating surfaces. The following sections describe the acquisition and processing of the survey data.

2.3.1 Acquisition

During 6 days in June 2015, a crew of 5 people acquired 14 km of multi-component seismic reflection data. This very efficient acquisition system consisting of vibratory source and an in-house developed landstreamer array can gather about 100 records per hour (Figure 9).



Figure 9 - Seismic reflection data acquisition in Kitimat. The vibratory source on wheels “minivib” is shown at the bottom left, towing the 100 m-long geophone array (landstreamer) which consisted of 72 sleds with 3 orthogonal geophones. All cables led to the command centre in the cab of the minivib.

For this survey, the minivib sweep length was 7.4 seconds long, with frequencies ranging from 20 to 280 Hz. The 140 kg mass vibrated in an in-line horizontal direction. The landstreamer consisted of 72 receiver sleds (each with 3 orthogonal geophones) spaced at 1.5 m. The distance from the source to the first geophone was 3 m. Sweeps were recorded every 4.5 m with a sampling rate of 1 ms.

A differential GPS (Novatel) mounted on the minivib was used to record coordinates and elevation along each survey line. Due to the dense tree cover at some locations, the altitude information was not precise and manual processing was required.

2.3.2 Processing

GPS elevation processing

The GPS elevation data required correction prior to topographic adjustment of the processed seismic profiles. This highest resolution elevation data available (2 m contours) was provided by the Township of Kitimat. Digital elevation model data (DEM) from the Province of BC had a coarser resolution (10 m).

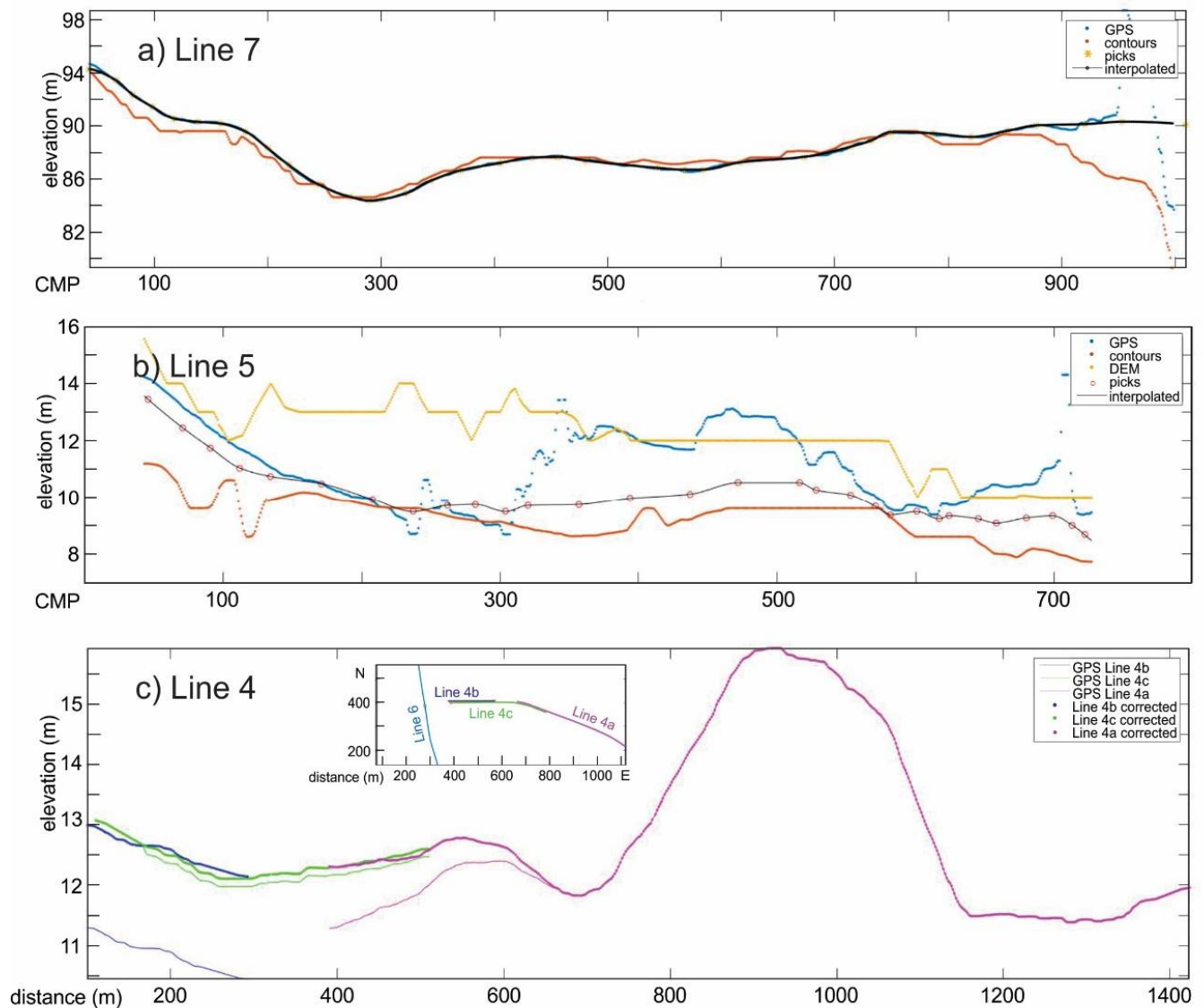


Figure 10 - GPS elevation data (blue dots in a) and b), and thin lines in c)) compared with provincial DEM (yellow line in b)) and township contour data (red line in a) and b)). The processing methodology to correct the GPS data (black lines in a), b), and c)) is explained in the text.

To process the elevation data, GPS, provincial DEM, and Township survey contour data were first compared to one another. A computer program was created for this purpose where the processor picks elevation points on the comparison image and the computer calculates a polynomial best fit to the picked points. Figure 10a shows an example of good GPS data up to the end of the line 7, where the signal is lost due to the tree coverage. Elevations from the township's contour data are shown in red, picked

points are shown as yellow stars, and the interpolated line is black. Note that line 7 is 2150 m long, with an elevation difference of 20 m the vertical exaggeration is more than 100.

Figure 10b shows an example of poor GPS elevation data (blue). It also shows the discrepancy between the provincial DEM (yellow) and the township contours (red). The “true” elevation is believed to be between the DEM and Township contours, hence points are picked (red circles) accordingly. Elevations are interpolated between the points shown by the black line.

An example of overlapping profiles is shown in Figure 10c. Lines 4 a, b and c were acquired on different days. Thin lines depict the collected GPS data. Corrections were made such that co-located points show the same elevations (dots/bold lines). The plain view of the overlapping lines is shown inset in Figure 10c.

Seismic processing

Table 3 shows the processing steps followed to create P-wave and SH-wave profiles (SH=horizontal component of the S-wave). Of particular interest are the velocity semblance analyses for both SH- and P-wave data, as well as the time to depth conversion; details are provided herein to describe these processing steps. Examples of the processing of Line 7 are shown throughout this section, but full profiles and time domain data are provided for all Lines in Appendix C.

Table 3. Processing steps and parameters.

Initial processing (all data)	
Format conversion, SEG2 to KGS SEG Y	
Spectral whitening	
Pilot trace based deconvolution	
Separation of V, H1, H2 components	
Applying of geometry	
Common Midpoint (CMP) sorting	
P-Wave V component	S-Wave H2 component
Frequency band pass filter (80-120-200-250 Hz) ⁺ (80-120-180-200 Hz) [□]	Frequency band pass filter (30-45-120-140 Hz) ⁺ (30-45-110-120 Hz) [□]
Frequency band reject filter (170-178-182-190 Hz) [□]	Frequency band reject filter (50-58-62-70 Hz) [□]
Scaling (trace normalization)	Scaling (trace normalization)
Bottom mute (S-, surface waves)	Top mute (P-, surface waves)
Velocity semblance analysis*	Velocity semblance analysis*
NMO corrections (~420-2050m/s)	NMO corrections (~150-760m/s)
Stacking, fold: 36	Stacking, fold: 36
Topography correction*	Topography correction*
Time to depth conversion*	Time to depth conversion*

* data provided in Appendix C

⁺ all lines except 5 and 6

[□] lines 5 and 6 only

Common midpoint (CMP) sorting

Minivib surveying with multifold coverage (multiple geophones and shot locations) produces large datasets with various source-geophone offsets. Processing sorted the data into common midpoint (CMP) gathers, which groups all the traces with a common midpoint together. Figure 11 shows a schematic of a common midpoint, which is the half distance between source and geophone. One CMP consists of several source-geophone pairs, which are sorted by increasing separation or offset. The number of traces/pairs belonging to one gather is called 'fold'. Depending on all the distances between sources and geophones, the fold is different. For this survey, the optimal CMP distance was 2.25 m with an average fold of 36, meaning that 36 traces are summed at one CMP location for best signal to noise ratio.

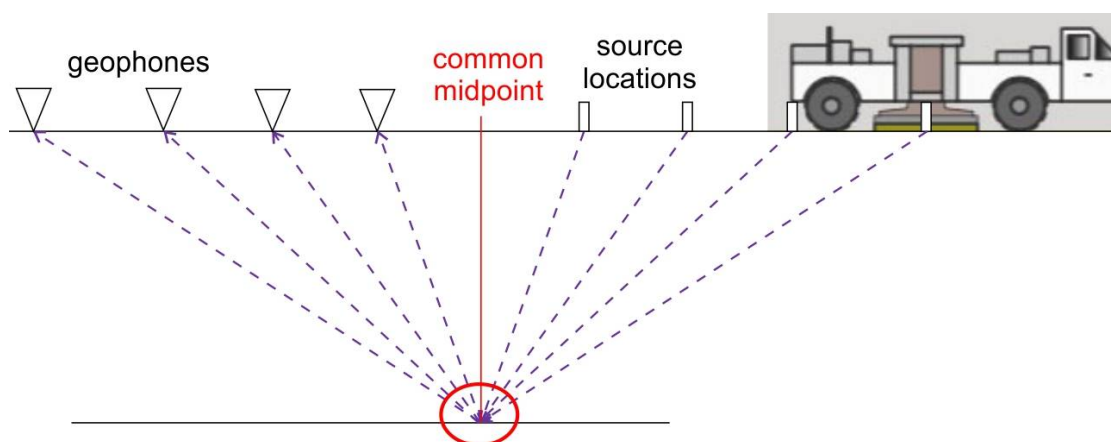


Figure 11 - Schematic showing the common midpoint (CMP) which is the half distance location between source/geophone pairs.

Velocity semblance analysis

At every 20th common midpoint (CMP) for P-wave and every 10th or 20th for shear waves, a velocity analysis was performed by calculating velocity semblance panels. High semblance values (green to red colours in Figure 12) indicate strong normal move-out (NMO) correction correlation for certain time/velocity pairs pointing to high amplitude reflections.

These time/velocity pairs (black crosses in Figure 12) are picked by the data processor. They are used for NMO correction before calculating one stacked trace per CMP gather. High semblance values relate to high amplitude reflections and to high impedance contrasts in the ground. Moreover, these time/velocity pairs provide first insights into the subsurface composition, as the velocities are equivalent to average velocities and the picked times can be converted to depth. An average velocity profile can be obtained by utilizing all analyzed CMP locations and interpolating in between the picked points.

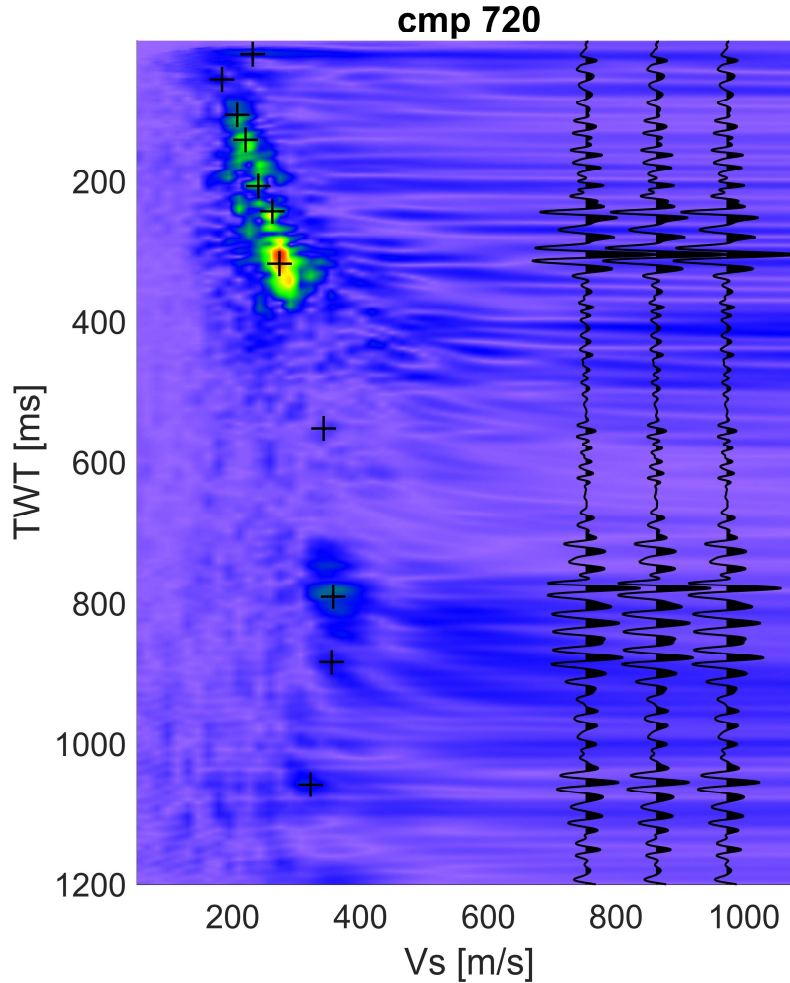


Figure 12 - Velocity semblance gather of Line 7, CMP 720. Green to red colors indicate high semblance values where time/velocity pairs are picked (black crosses). The resulting stacked trace after NMO correction using these time/velocity pairs is shown three times overlaid on the panel to emphasize the intervals of high semblance values.

Figure 13 (panels A and B) show average velocities of Line 7 based on the semblance processing. Note that the interpolation algorithm produces “islands” of low and high velocities which are artefacts.

Average velocities are used to calculate smoothed interval velocities (Dix, 1955, Pugin et al, 2013) shown on panels C and D of Figure 13. Interval velocities are very sensitive to rapid vertical changes. Especially for thin layers, velocities can be very high or very low. They can also alternate from low to high very quickly in the vertical direction depending on layer thickness and average velocity gradient (compare CMP 820 at the bottom of Figure 13). These vertical velocity variations should not be over-interpreted.

For each seismic profile, digital files of average and interval velocities are provided in Appendix C. The columns contain the following information: CMP number, time in ms, depth in meters, average velocity in m/s and interval velocity in m/s.

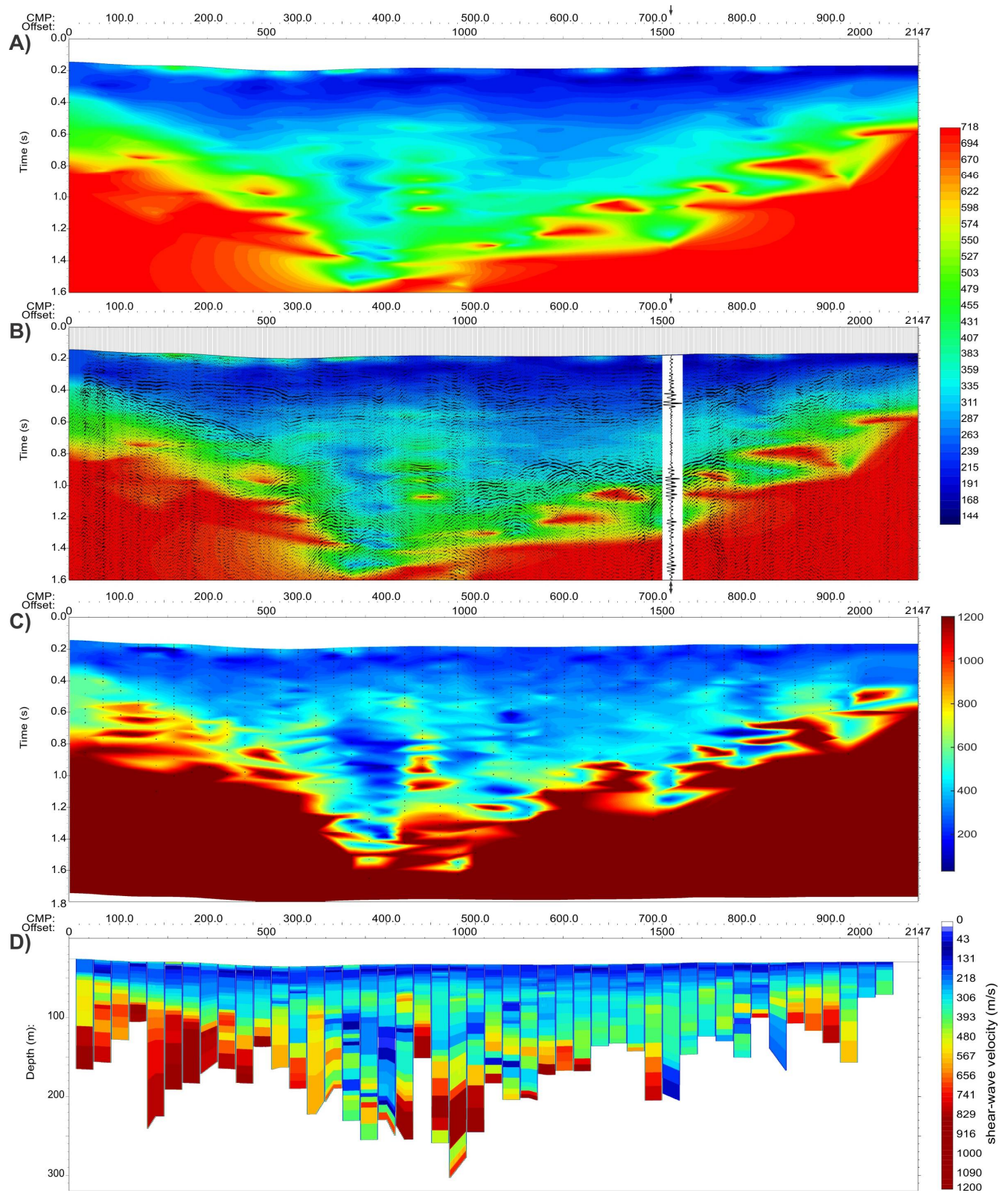


Figure 13 - A) Interpolated average shear wave velocity profiles from Line 7. B) The interpolated average shear wave velocity shown overlying S-wave seismic traces. The arrow locates CMP 720 (shown in Figure 12). C) Interpolated interval shear wave velocities are shown with locations of the semblance picks (bold points) and interpolated points in between which are used for the interval velocity calculation. D) shows velocity columns for analyzed CMPs in depth domain with no interpolation.

Time-to-depth conversion

Ideally, borehole shear wave velocity measurements are used for the time-to-depth conversion of the seismic time domain profiles. In Kitimat, shear wave velocities were only available for the hospital site (Figure 3) and BH06 (Figure 8) which are both too far from the seismic profiles to be used directly. Therefore, the interval velocities calculated from the semblance analyses were used to build a simplified velocity depth model. Looking at the velocity complexity in Figure 13, it is clear that not one single velocity-depth function will fit the whole length of the profile. On the other hand, using all velocity-depth functions from the CMP semblance analyses displays too much detail and leads to unsatisfactory results for a time-to-depth conversion. Hence, the interval velocity profile was divided into regions (groups) with reasonably similar velocity structures (Figure 14, top panel). For each region, a best fitting curve is calculated based on a power law curve in the form of $V_s = a + b * t^c$, where a , b and c are fitting coefficients and t is two way travel time in ms. This curve fitting analysis follows a similar approach taken by Hunter et al. (1998). These curves were used to create a model with a 30 CMP wide transition between the regions. 30 CMPs provided a good compromise between retaining detail (not masking narrow regions) but providing some smoothing in complex velocity regions. Figure 15 shows the resulting time-to-depth conversion model of Line 7 using the curves shown in Figure 14.

The calculation of best fitting curves as described above was automated such that the effect of different regions can be compared and a simple, well-fitting model can be selected. This procedure is performed for P- and S-wave profiles separately. Note that there is a linear interpolation between the nodes in time and along the profile.

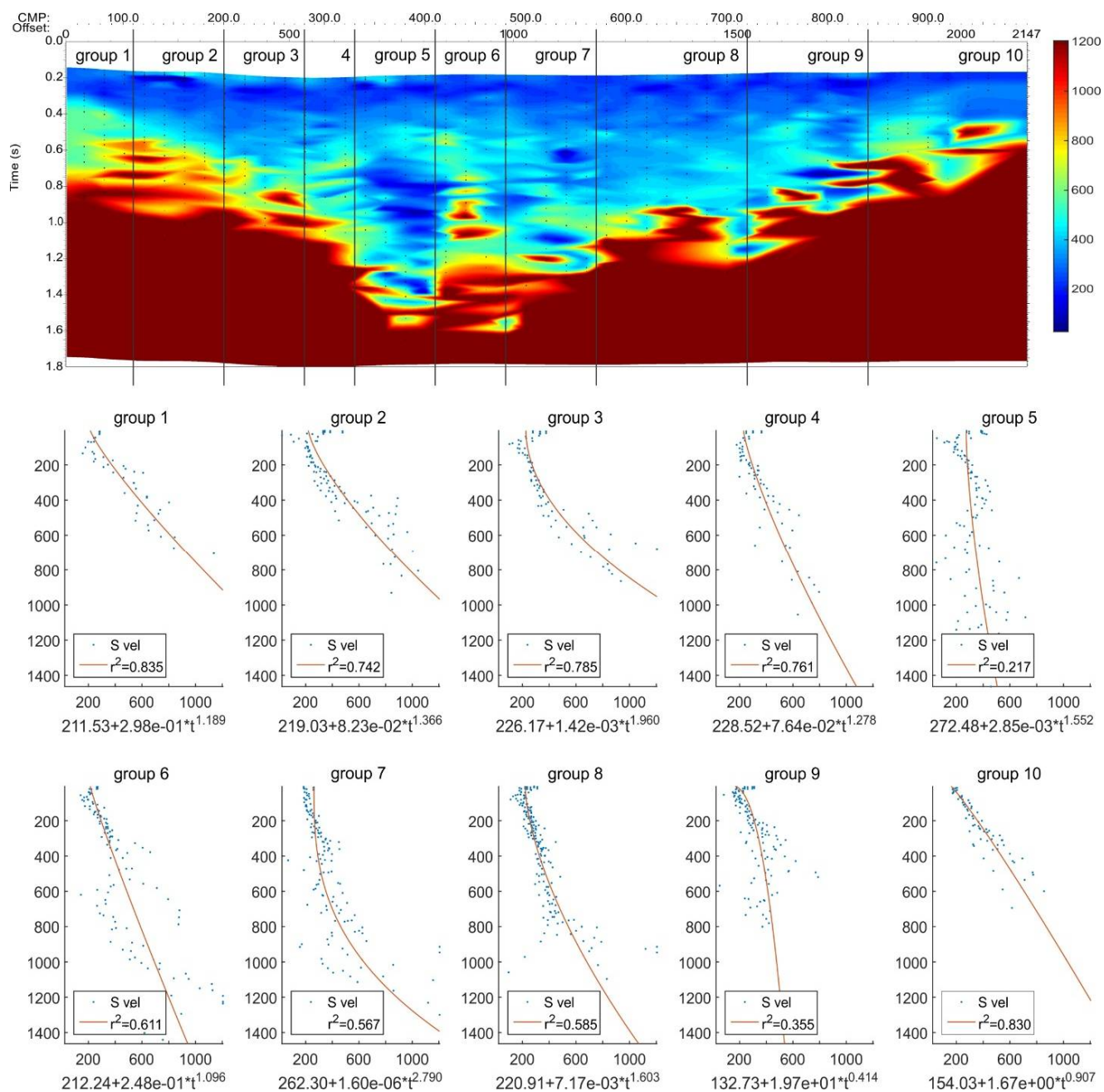


Figure 14 - Creating a shear wave interval velocity model for Line 7: Interval velocity-time pairs (black dots) are grouped into regions (top). Interval velocity-time pairs (blue dots) are shown with the calculated best fitting curve (bottom). Coefficients are shown below each group.

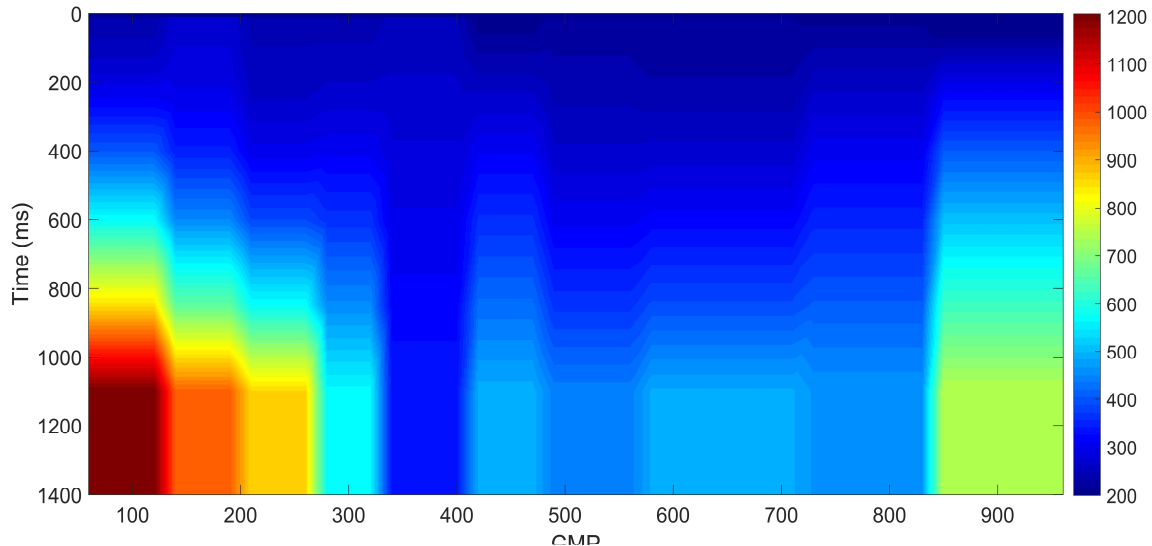


Figure 15 - Shear wave velocity model (in two-way-travel time) for Line 7 obtained from the region grouping and best fitting curves from Figure 14.

3.0 Results and Interpretation

At any given depth, the range of interpreted shear wave velocities in the sediments overlying the bedrock in Kitimat is broad and can vary rapidly, reflecting the wide range of material types (clay-sized grains to boulders) and depositional environments (marine, glacial, alluvial) found in the study area. Figure 16 presents an example of this range, showing processed shear wave velocities from seismic Lines 4 and 7 alongside seismic cone penetrometer data from the hospital site (CPT97-06, “Hospital SCPT”), and downhole shear wave velocities from the Kitimat landfill (BH06). By way of comparison, a V_s -depth curve from the Fraser River Delta sediments (Hunter et al. 2016) is plotted alongside the Kitimat V_s data. The V_s in the silts and clays from the upper 45 m of the hospital site compares favorably to the Fraser River Delta curve in the same depth range. In contrast, velocities from BH06 are much higher in the sands and gravels of a river terrace, clearly indicating the variability (and complexity) of seismic facies within the Kitimat area.

In addition to velocity ranges, categorizing seismic facies provides a second approach for interpreting reflection profiles. Facies were based on variation in reflection

- strength (amplitude), from transparent to very high,
- coherency, from very chaotic to very continuous, and
- structure, from dipping, to parallel, to combinations (e.g, onlap/offlap).

Table 4 summarizes the main characteristics (velocity ranges and facies) observed in the Kitimat profiles.

When available, water well information was used to calibrate the depth of seismic reflections and plotted on the seismic profiles with simplified lithologies indicated (see Table 1).

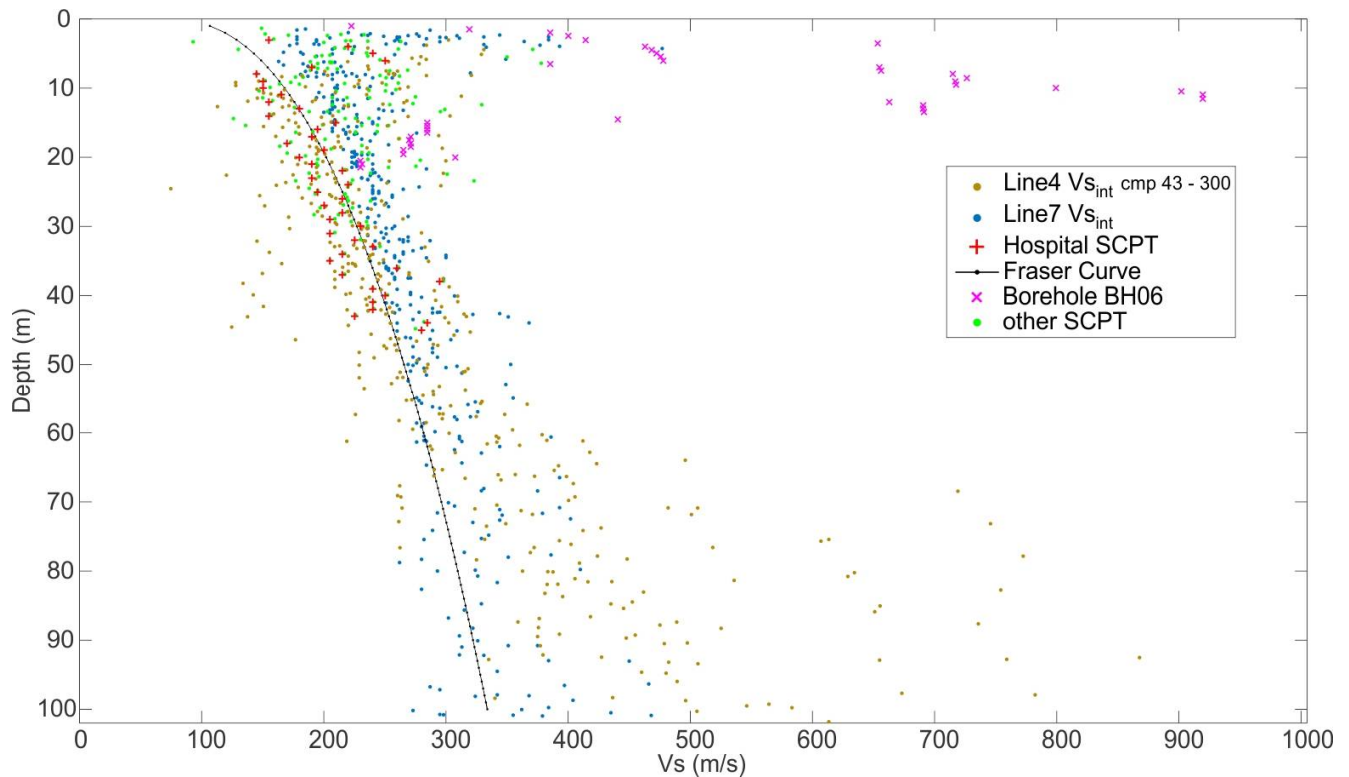


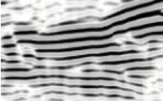
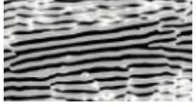
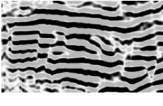
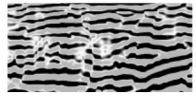
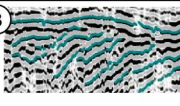
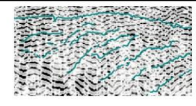
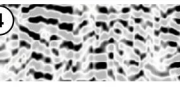
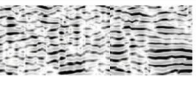
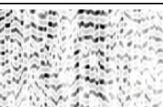
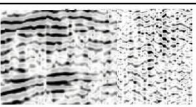
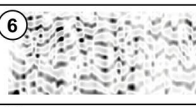
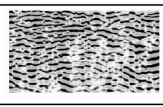

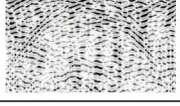
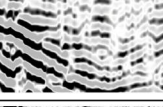
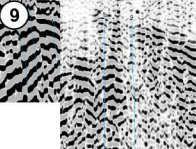
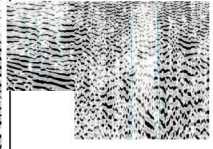
Figure 16 - Range of shear wave velocities encountered in the Kitimat study area, compared to the Fraser River Delta Vs curve from Hunter et al. (2016).

Seismic Profile Interpretation

In the context of these facies categories (Table 4), a short description of the seismic profiles is given below, with an interpretation of subsurface conditions. Refer to Figure 2 for the line locations, and to Appendix C for the detailed raw and interpreted profiles, as well as interval velocities. All profile figures in Appendix C show P-wave sections on the left and S-wave sections on the right. The top profiles present seismic data in time domain (two-way travel time). Seismic interval velocity obtained from velocity analyses is shown superimposed on reflection data in the time domain on the second panel, and the third panel shows the same velocities after conversion to depth. The fourth panel shows the interpreted reflection data in depth. All depth axes show elevation in m above sea level (asl) and the vertical exaggeration is 2. The inset map at the base of each figure shows the profile location with CMP numbers indicated. Exact CMP location coordinates in UTM can be found in Appendix C.

The figures also present horizontal-to-vertical spectral ratios (HVSr's) calculated from the microtremor recordings along the seismic lines. The maximum of this ratio curve (peak) is shown after conversion from frequency to two-way travel (TWT) time and transformation to depth using same velocity depth model as the seismic TWT profiles. Because an empirical function relating active (reflection seismic) and passive (HVSr) fundamental periods has not yet been established (e.g. Hunter et. al 2010), the presented HVSr peak depths exhibit an unknown error. Further research on this issue is ongoing. Correlation with the bedrock surface is poor; the seismic profiles show that the impedance contrast identified most commonly by the microtremor recordings is an intra-sedimentary horizon.

Table 4. Overview of seismic facies and velocities for interpreted lithology.

facies example P	facies example S	amplitude strength	coherency	structure	min Vs	max Vs	SCPT + BH Vs	dominant material	comments
① 		very high	very high	parallel		1200 +		bedrock surface	- usually strongest reflection - usually better observed on P
② 		high	medium to high	1) foresets	400	800		diamicton	- might be hard to distinguish from bedrock - might or might not show internal structure
③ 		medium to high	chaotic to high	1) foresets	300	500	380-920 ²	gravel	- most variable facies - most variable velocities - most variable material (pebble size, sorting)
④ 		weak to medium	chaotic to high	1) foresets parallel	250	450	200-900 ² 190-360 ³ 130-260 ⁴	sand	
⑤ 		medium	medium to high		150	300	160-330 ³ 170-260 ⁴	silt	- dominated by silt-sized particles
⑥ 		P: low S: medium	P: low S: medium			≤200	260-270 ² 100-230 ³	clay	- dominated by clay-sized particles - velocity increases as a function of depth
⑦ 				diffraction					- might stem from boulder, fracture, lateral discontinuity, bottom of steep bowl
⑧ 				onlap					
⑨ 				lateral discontinuity					

¹⁾ might or might not show structure

²⁾ BH06 (only 25 m deep)

³⁾ SCPT (compare Figure 3)

⁴⁾ Fraser Delta (Hunter, 2016)

Seismic facies can have different expressions when they are obtained from P-wave (vertical) versus S-wave (horizontal) reflections. For example, silt and clay often exhibit coherent, horizontal reflections on the S-wave but very chaotic, transparent reflections on the P-wave. When the two components are interpreted together, they provide more information on material types and unit boundaries. On the figures in the following section, both components are shown, and reflections are highlighted on the components where they are observed. A combination of all interpreted reflections is provided on the figures of Appendix C.

Line 5

The southernmost Line 5 (Figure 17) exhibits a strong reflecting horizon dipping towards the south. The strong P-wave amplitudes suggest this reflector is most likely associated with facies 1, and the horizon is interpreted as bedrock. Reflection amplitudes and velocities (facies 2, 3) in the sediments draped above the bedrock are interpreted as gravel or diamicton. The velocity decreases upwards, suggesting a fining upward trend interpreted as sand to silt and clay. The upper-most shear wave velocities are in the same range as those measured at the near-by hospital site SCPT (silty-clayey to silty-sandy sediments). There are notable differences in facies between P- and S-wave profiles. For example, the mound near the northern end of the profile shows internal structure on the P-wave profile, whereas the S-wave profile shows more transparent facies (facies 3) which is consistent with coarse material, potentially a gravel bar. The upper part of this mound shows a lower velocity which might indicate a sandy horizon. An erosional surface is visible on the S-wave profile at the top of the mound dipping north towards the northern end of the line. The southern half of the profile from bedrock up, exhibits internal structure of low to medium amplitude reflections (facies 5) interpreted as fine sand/silt with sand and gravel lenses. All four microtremor recordings on Line 5 clearly image an impedance contrast within the sediments, which is interpreted as a horizon between sand/gravel and silt.

All this is interpreted as evidence for a meandering river in an alluvial plane with high energy deposits (e.g. gravels) in the north, erosion on the north flank and perhaps on the south side where it is possibly covered by sand. Lower energy deposits at the southern end of the profile may include sand deposits which fine upwards into silt.

Line 6

The south end of Line 6 (Figure 18) starts parallel to Line 5 (around CMP 320). The bedrock surface is irregular and poorly defined by reflections on the S-wave profile. On the P-wave profile however, there are medium to high amplitude continuous reflectors (facies 3). A deep trough is visible at CMP 920 before a surface, interpreted as bedrock, rises steadily towards the northern end of the line, just west of the bedrock dome identified on the surficial geology map (

Figure 4). Bedrock was confirmed about 20 m below surface in near-by water well 13675. Possibly, a large boulder was misinterpreted for bedrock. The microtremor measurement 40 m further south shows a clear peak correlating quite well with the dipping gravel surface imaged in the seismic profile. This mud-gravel contrast possibly creates the strong resonator measured by the microtremor record. On top of the bedrock is a high velocity unit (interpreted mainly as a mixed gravel layer) of varying thickness, reaching greatest thickness (about 150 m) around CMP 900. The P-wave section shows a well defined internal structure with southward dipping layers. These layers are likely associated with foresets which are fining upwards as the slowing velocities indicate. On the shear wave profile these foresets are not as clearly defined. On the other hand, the silt and clay layer at the surface is much better resolved on the S-wave profile. Besides the northernmost microtremor measurement, the other six recordings show peak amplitudes considerably above the bedrock surface which seem associated with depositional changes in the sediments.

Line 6 correlates well with features observed in Line 5, as the profiles cut through an alluvial plane at different angles.

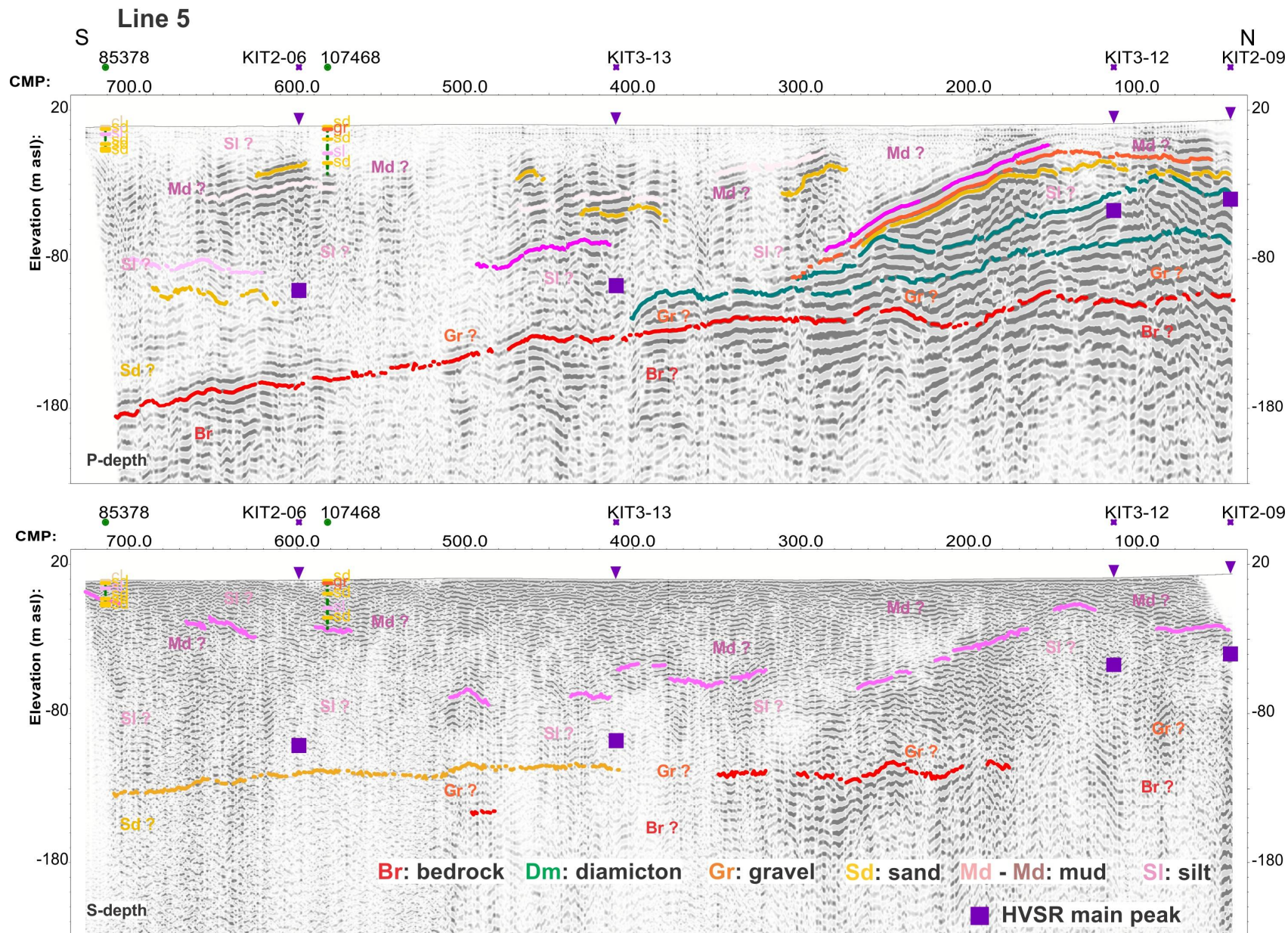


Figure 17 - Interpretation of Line 5 with highlighted P-wave reflections on P-wave depth-converted section on top and highlighted S-wave reflections on S-wave depth-converted section at the bottom. The vertical exaggeration is 2.

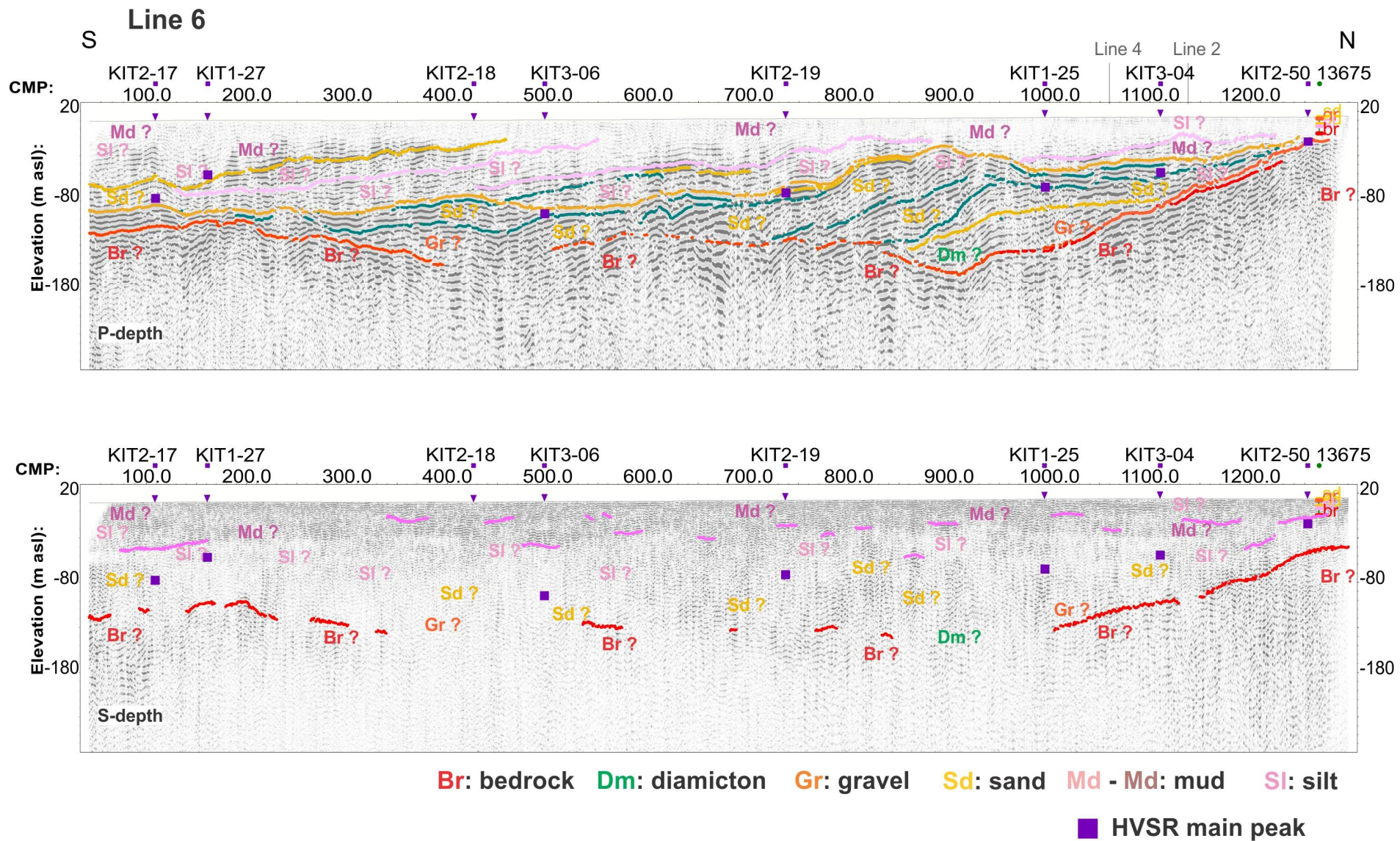


Figure 18 - Interpretation of Line 6 with highlighted P-wave reflections on P-wave depth-converted section on top and highlighted S-wave reflections on S-wave depth-converted section at the bottom. The vertical exaggeration is 2.

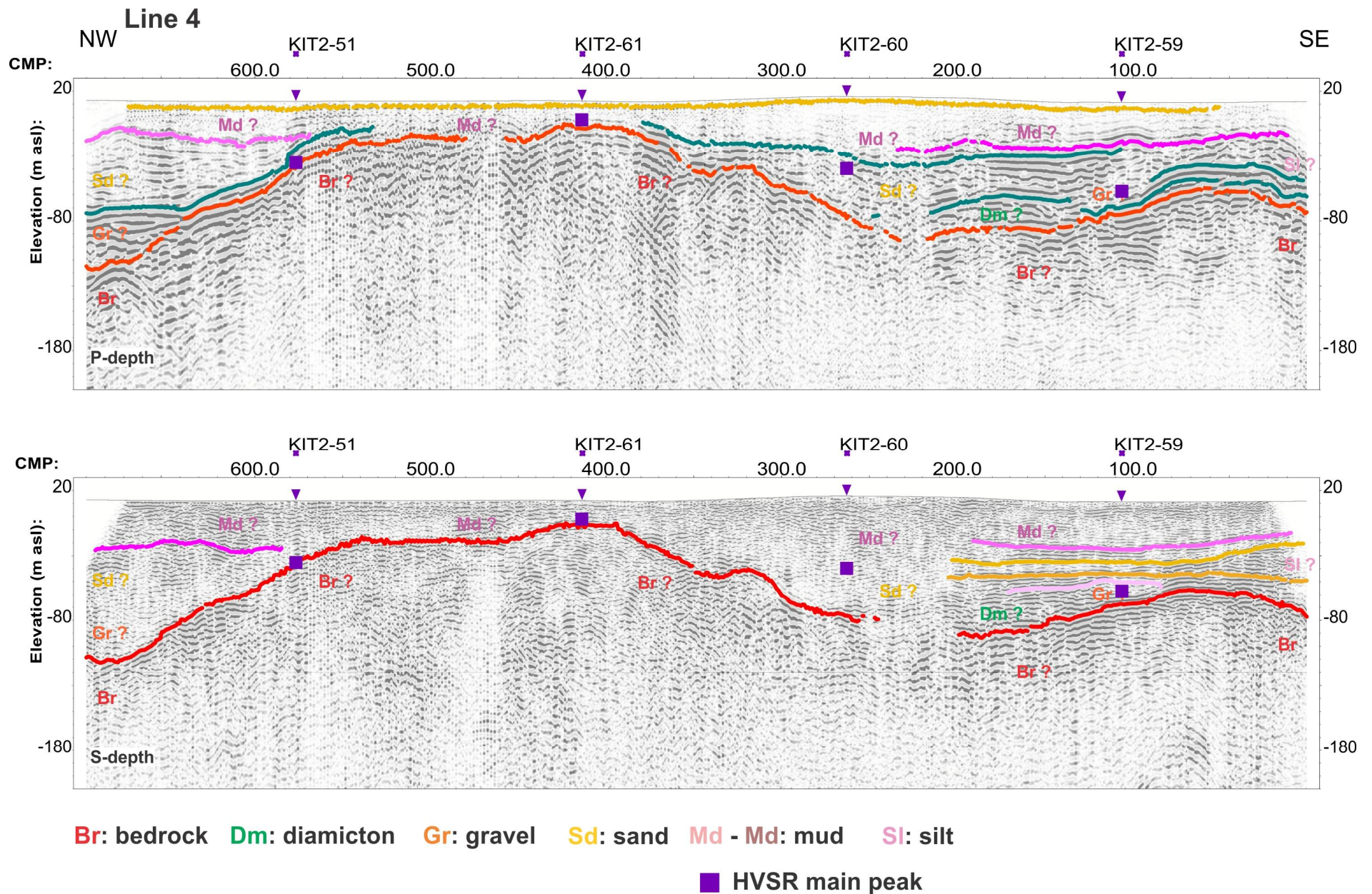


Figure 19 - Interpretation of Line 4 with highlighted P-wave reflections on P-wave depth-converted section on top and highlighted S-wave reflections on S-wave depth-converted section at the bottom. The vertical exaggeration is 2.

Line 4

The western half of Line 4 (from approx. CMP 600 to 350, compare Figure 19) displays the southward continuation of the outcropping bedrock dome further the north. The bedrock surface rises steeply in the west and more irregularly in the east and has a second bump near the eastern end of the profile. Here, high amplitude, continuous reflections overlying bedrock indicate well stratified sediments of seismic facies 2 or 3 (diamicton or gravel). Velocities and facies suggest overlying materials fine upwards to sand and silt. Around CMP 210, the reflections become more chaotic both for P- and S-wave sections. On the western side of the bedrock ridge, sediments can be divided into 3 layers: the first (and deepest) shows strong reflections on the P-wave profile and more transparent reflections on the S-wave profile best described by seismic facies 3, suggesting coarse material overlying bedrock. Weaker reflections (facies 4) suggests sandy layers in the center. Weak P-wave coherence with stronger S-wave coherence in the upper layer fits facies 5 and 6 and is interpreted as silt or silty-clay at the surface.

The peak amplitudes of two western microtremor measurements match bedrock at the ridge quite well. On the eastern side however, peak amplitudes correspond to impedance contrasts within the sediment column.

Line 2

Line 2 (Figure 20) is a westward continuation of Line 4, starting around CMP 1140 of Line 6, and ending at the Kitimat River. The bedrock surface is hardly recognizable on the eastern side of the profile. It is very discontinuous and might be interpreted near CMP 150 at an elevation of -160 to -180 m. At the western side of the profile a strong contrast (interpreted as bedrock) is identified at an elevation of about -130 m which is higher than the strong impedance contrast (peak) in the microtremor measurement. Material velocities suggest bedrock is overlain by gravel or diamicton (facies 2, 3), followed by gravelly sand (facies 3, 4) and fine sediments (facies 5) in a fining upward sequence. At the eastern end of the line, on the P-wave profile, distinct onlaps are visible at the sand-mud boundary at -20 to -50 m elevation. The most interesting feature is located near CMP 150, where a discontinuity is visible both on P- and S-wave profiles. The highlighted topmost reflection is vertically offset by about 30 m. A distinct zone of lower amplitudes can be seen on the S-wave profile being capped by muds about 20 m below surface. This may indicate the presence of an ancient fault, interpreted as inactive due to lack of offset (disturbance) observed in younger overlying sediments. This interpreted fault may trend N-S as it cannot be seen on Line 6 or Line 1.

The peak amplitudes of two eastern microtremor measurements correspond to intra-sediment contrasts, interpreted as silt/mud overlying gravel/sand.

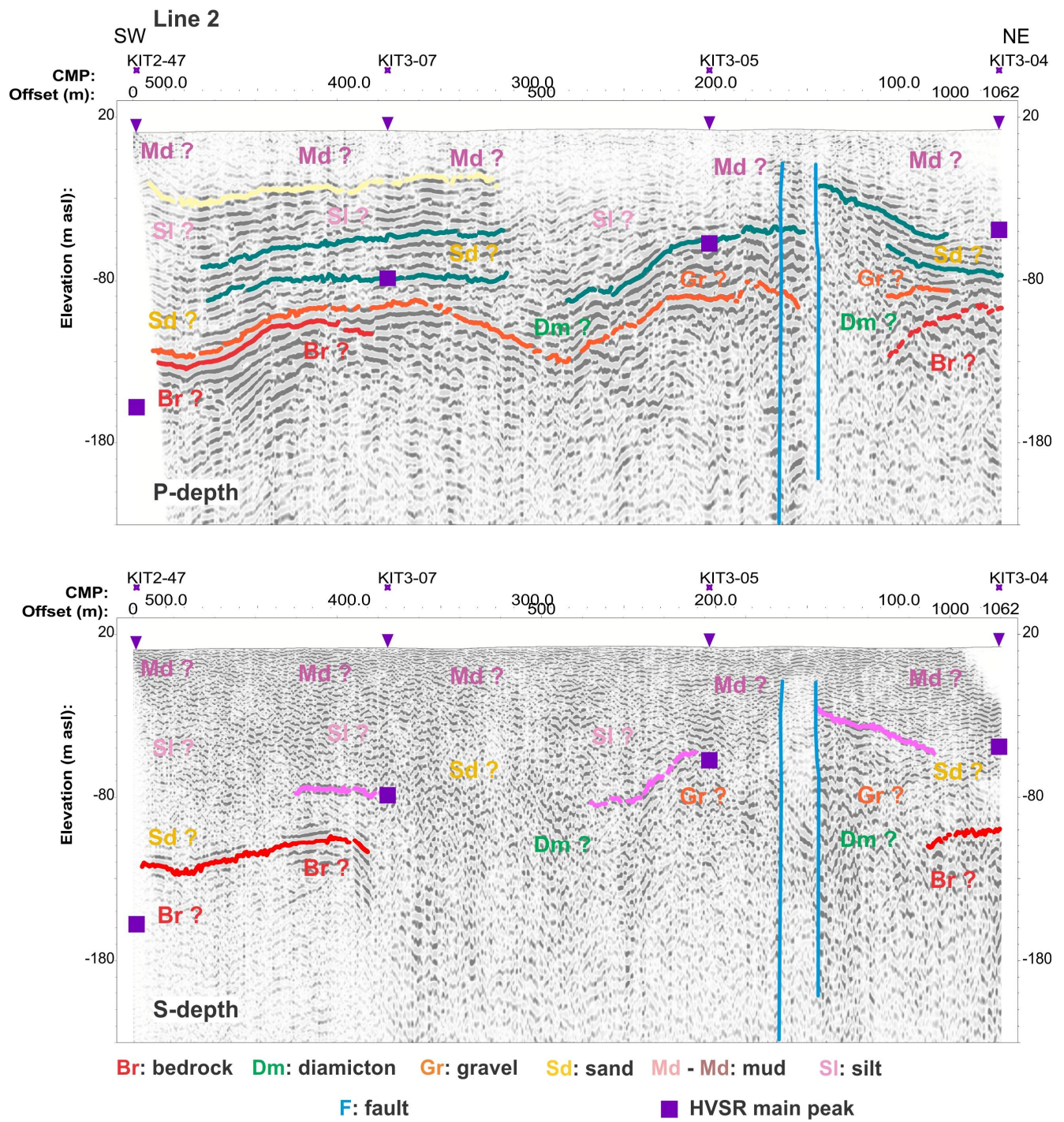


Figure 20 - Interpretation of Line 2 with highlighted P-wave reflections on P-wave depth-converted section on top and highlighted S-wave reflections on S-wave depth-converted section at the bottom. The vertical exaggeration is 2.

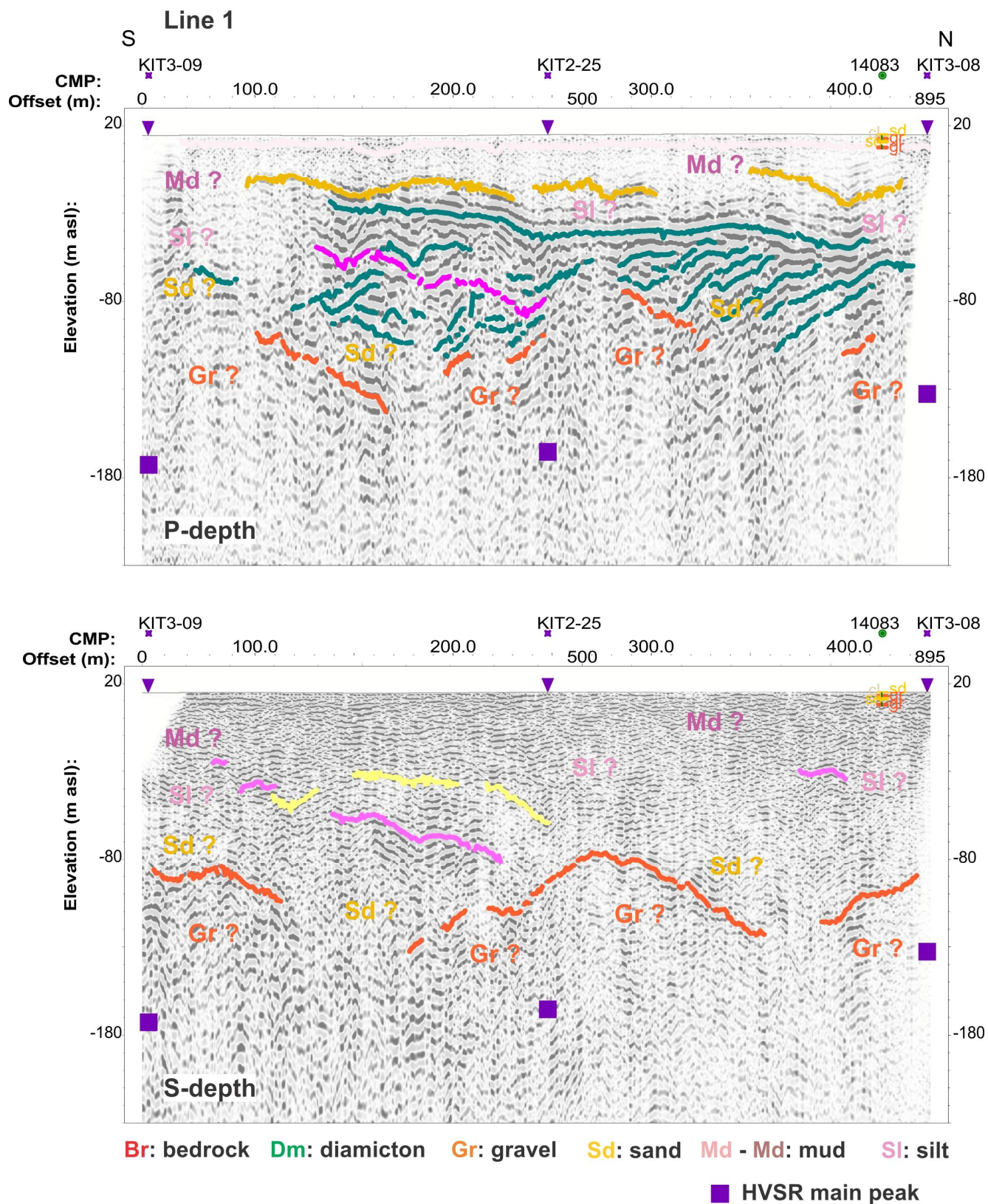


Figure 21 - Interpretation of Line 1 with highlighted P-wave reflections on P-wave depth-converted section on top and highlighted S-wave reflections on S-wave depth-converted section at the bottom. The vertical exaggeration is 2.

Line 1

On Line 1 (Figure 21), a deep reflector (bedrock) cannot be resolved from P-wave energy and is only visible in certain places - but not interpreted - on the S-wave seismic section. Chaotic, high amplitude reflections (facies 3) lead to an interpretation of a gravel layer of varying thickness overlying bedrock (undulating between -90 and -140 m asl). Coarse sand may fill the gravel troughs and cover the gravel hills. Two sequences of gravel (or sand?) divided by an erosional surface are interpreted in the southern half of the section. Reflections indicate both sequences show clear internal structure with foresets predominantly dipping to the south. Reflection amplitudes and material velocities (facies 5,6) and sediment structure suggest that fine sand or silt is covering the channel fills and mud or silt forms the surface layer.

Three microtremor measurements situated on this profile indicate a strong impedance contrast, which corresponds to a depth of roughly 200 m below surface at the southern end of the line rising to about 150 m below surface at the northern end. While this reflecting surface is not visible in the seismic profiles, it is interpreted as a possible bedrock surface.

Similarly to Lines 2, 4, 5, and 6, Line 1 also shows evidence of an alluvial plane with gravel bars and gravel/sand foresets covered by silt.

Line 3

Line 3 (Figure 22) is an east-west profile following the main highway through town, from City Center eastward toward a residential area atop a plateau. The material underlying the ridge has been interpreted as a morainal ridge by Clague (1977). The eastern end of the profile turns off the highway and follows the Kitamaat Village Road down towards Minette Bay. Bedrock is interpreted on the P-wave section only at the very western end of the profile (facies 1), where a rock dome outcrops to the north. It is somewhat clearer on the S-wave profile, where bedrock is interpreted to undulate between -30 and -150 m before plunging to probably -330 m at the eastern end of the profile. Velocities and reflection amplitudes (facies 3, 4) suggest this very deep trough is likely filled with massive gravel and/or sand, perhaps stemming from high volume flow of a glacial river. Bedrock depressions are generally filled with high velocity materials (facies 2, 3: gravel or diamicton) which could be up to 50 m thick (e.g. CMP 730). Sand and silt wedges overlie the western half of this profile where S-wave reflections are fairly continuous (facies 4, 5). On top of this layer sits a massive layer of variable material with some internal structure. It is about 30 m thick at the western end and increases in thickness to about 160 m as the profile climbs up the ridge. This is thought to be the drift package as described by Clague (1977). At CMP 240 of the eastern end of the profile, there are multiple erosional surfaces visible on the P-wave profile and a deeper one on the S-wave profile. The deeper channels seem to be filled with sand whereas the shallower ones are likely filled with silt and mud. This erosion might be associated with an earlier tributary flowing directly into Minette bay.

The microtremor measurements show peak amplitudes considerably above the bedrock surface, and seem associated with depositional changes in the sediments and the erosional surfaces, particularly evident at the easternmost recording site.

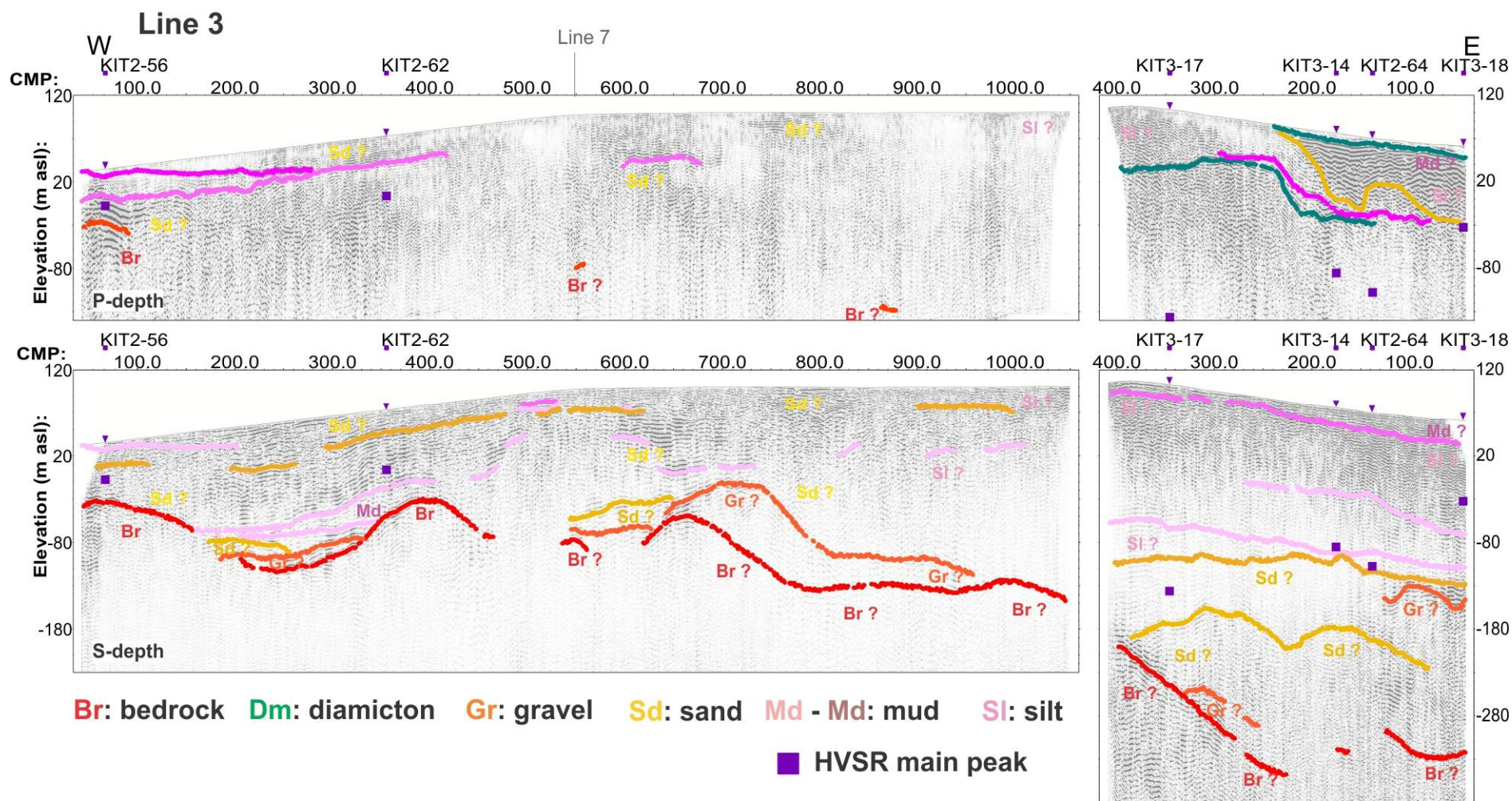


Figure 22 - Interpretation of Line 3 with highlighted P-wave reflections on P-wave depth-converted section on top and highlighted S-wave reflections on S-wave depth-converted section at the bottom. The vertical exaggeration is 2.

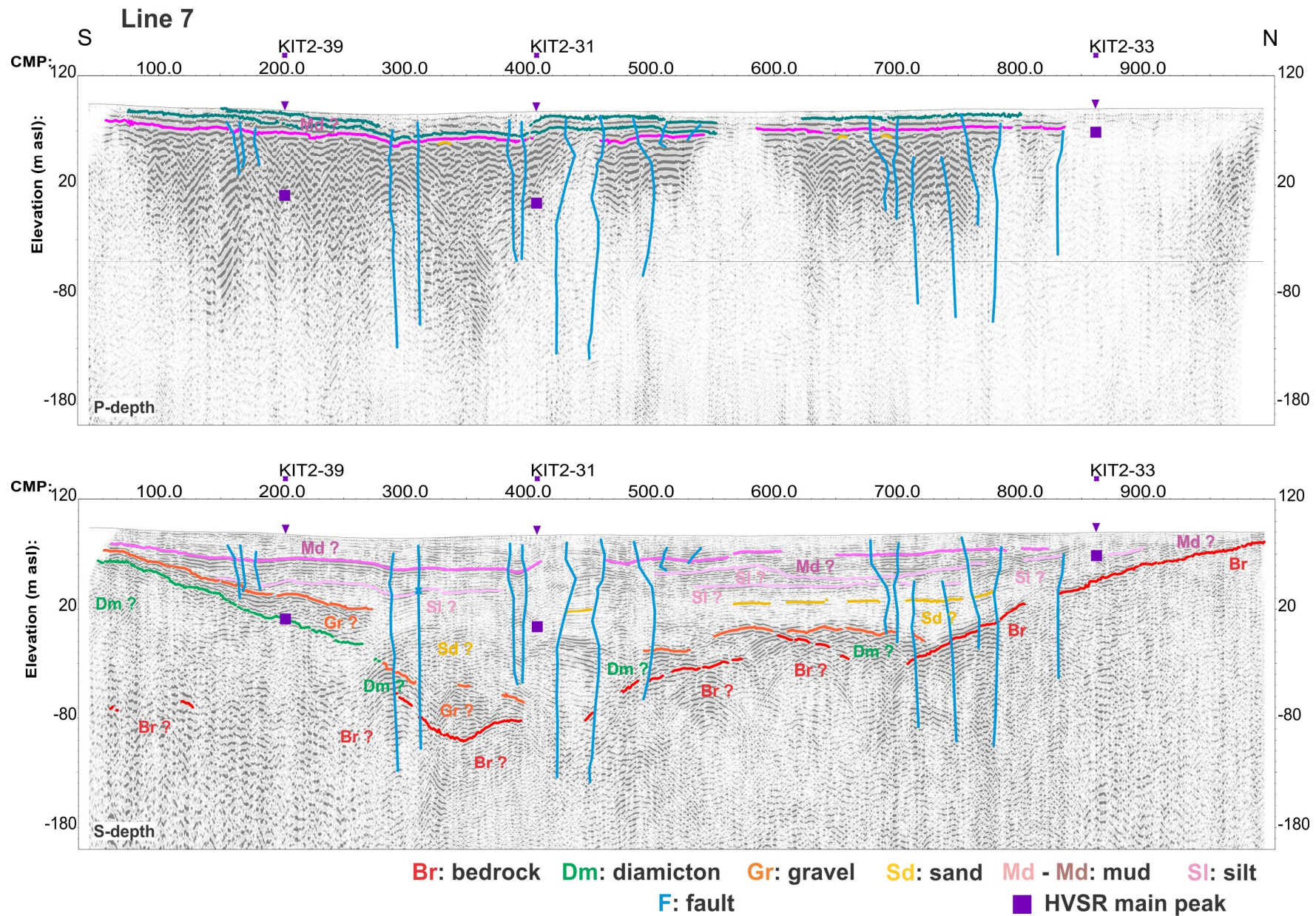


Figure 23 - Interpretation of Line 7 with highlighted P-wave reflections on P-wave depth-converted section on top and highlighted S-wave reflections on S-wave depth-converted section at the bottom. The vertical exaggeration is 2.

Line 7

Line 7 (Figure 23) is situated in the residential community atop a plateau. Clague's 1977 surficial geology map indicates marine silts and clays are present at surface, observed at the time of this survey at an excavation site (Figure 5a). The profile starts about 100 m north of CMP 550 on Line 3 trending NE up to CMP 450 before curving to NW from CMP 600 to 750. From about CMP 800 it trends northwards.

As in Line 3, a strong impedance contrast representing the bedrock surface is not visible on the P-wave profile and is barely recognizable on the southern part of the S-wave profile despite the presence of highly reflected seismic energy. This implies there is very little V_s contrast between the drift and the bedrock surface. For P-waves most of the energy is reflected at shallow depths in the sediment column before reaching bedrock. The deepest horizon interpreted as bedrock is found around CMP 350 and it rises irregularly to the north where an outcrop was observed during the field work just beyond the end of the seismic line. Several diffractions (facies 7) stem from the irregular bedrock surface as observed in the center of the S-wave profile. In the south, bedrock is covered by about 130 m of thick glacial drift as described for Line 3. This drift slopes northwards and probably extends to cover the bedrock trough up to CMP 760. It is difficult to differentiate the seismic signature of diamicton and gravel (facies 2 and 3). On top of this high amplitude package there is a layer interpreted as sand (facies 4) with a rather flat top marked at about 25 m asl. It is possible that sand continues to 35 m asl, where the transparent facies are replaced with medium amplitude, continuous reflections (facies 5, 6) indicative of silts and muds. Interestingly, a depositional change within the mud-silt layer creates a very strong impedance contrast on the P-wave section. Several diffractions (facies 7) can be seen originating at this boundary. Many zones of vertical offset were observed in the sediment (marked as blue lines), where vertical displacement and/or abrupt changes in reflection strength are visible. These features, tentatively interpreted as faults or fracture zones, are either associated with glacial rebound or neotectonic faulting, as some of these faults seem to continue into the bedrock.

All three microtremor recordings measured along the profile show peak amplitudes considerably above the interpreted bedrock surface. At the northernmost site, the peak amplitude correlates well with the boundary that creates the strong P-wave impedance contrast. The southernmost site displays a peak at the top of the glacial drift package, and the central site shows a peak close to the gravel-sand boundary.

4.0 Conclusions

A series of geophysical surveys were conducted within the town of Kitimat to investigate the potential for amplified site response to earthquake shaking. Surface and downhole seismic surveys were conducted to quantify the ranges of shear wave velocities in the different sediment types, and image sediment structure. HVSR curves were computed from microtremor recordings along the seismic lines and across the town to measure resonant site frequencies (the frequency at which earthquake energy is most amplified). The seismic profiles and HVSR curves were compared to determine if a common stratigraphic horizon is causing a strong site resonance. The results indicate no single geological horizon across the site is attributable to the main resonating surface interpreted in the HVSR curves.

Seismic sections indicate a complex sedimentary structure with a wide range of material velocities and seismic facies, from massive, to highly reflective, to scattered and chaotic. These responses reflect a range of material types (clay-sized grains to gravel and boulders) and depositional settings (marine, glacial, alluvial systems). Profiles also reveal a highly irregular bedrock surface (where resolvable), thus

dispelling the concept of smooth walled, 'U'-shaped basin. To assist in the interpretation of stratigraphy, nine seismic facies were described which were based on material velocity, reflector amplitude, and coherency (continuity).

When deeply buried under dispersive or diffractive sediments (tills, gravels, boulders, sands), reflections from the bedrock surface were difficult to resolve. The base of the center of the valley could not be resolved. Seismic depth sections suggested the bedrock surface could be several hundreds of meters deep, as seen along the Kitamaat Village Road near Minette Bay (Line 3), reaching nearly 400 m deep. However, the interpreted bedrock surface undulates, and shallows as it approaches the outcropping rock dome near the center of town on Haisla Blvd.

The position of the seismic lines within the valley influenced the near-surface stratigraphy interpreted in the seismic sections. Lines 1, 2, 4, 5, 6, and the end of Line 3 are interpreted to contain features observed in alluvial plane settings such as gravel bars and sand/gravel foresets, covered by silt. Line 3 reveals a drift package as described by Clague (1977), but which shows evidence of structure, potentially a raft of glacially transported material, or an ancient slide or slump from valley sides. Line 7 reveals a valley flanked by the moraine to the south and bedrock to the north, filled with sands and gravels, and capped with approximately 50 m of marine sediments (silts and clays). Numerous high amplitude diffractions at the base of the valley reveal a chaotic surface of boulders/gravel or bedrock.

Offsets in sediments are visible in Lines 2 and 7. Faults, interpreted as inactive or a result of past glacial tectonics are identified on the sections. Any evidence of recent sediment disturbance caused by earthquakes could not clearly be resolved in the profiles.

An important aspect of this work was using the seismic profiles to develop an understanding of the relationship between the HVSR peaks and the underlying stratigraphy. The resonant frequency (or period) rarely corresponded to the bedrock surface unless the bedrock was shallow (e.g. Line 2). Most commonly, the peak is related to an intra-sedimentary reflector and depended strongly on the velocities of the sediments and the topography of the resonating surface. Of note on Line 1, the peak indicates a resonating horizon (bedrock?) deeper than all other horizons resolved by seismic. In this complex sedimentary setting, the HVSR peak is shown not to be responding to one common geological horizon.

The results of the seismic analyses are providing input for the next steps of the study, which involve developing a cross sectional model of the valley for ground motion modeling.

5.0 Acknowledgements

The authors wish to thank the District of Kitimat for their support in providing geotechnical reports, elevation data, permission to survey public roads, and support during the survey. We also wish to thank the Ministry of Transportation in British Columbia (MTBS) for permission to survey along the Kitamaat Village Road. Finally, we thank land owners Jack Oviatt and RioTinto for access to their roadways for survey Lines 5 and 6, respectively.

6.0 References

- AGRA, 1997. Kitimat Health Care Centre: Geotechnical Assessment, Report prepared for the District of Kitimat; 20p. + appendices
- AMEC, 2010. Preliminary geotechnical report, proposed Kitimat Terminal, Enbridge Northern Gateway Project, Kitimat British Columbia, Report prepared for Northern Gateway Pipelines Inc by AMEC Earth & Environmental, submitted on September 9, 2009 and revised on March 26, 2010. File No. EG0926008.4200, 188 p. https://docs.neb-one.gc.ca/ll-eng/llisapi.dll/fetch/2000/90464/90552/384192/620327/624798/619886/B1-18_-_Vol_3_%E2%80%93_Gateway_Application_%E2%80%93_Engineering%2C_Construction_and_Operations_%28Part_14_of_19%29_-_A1S9Z1.pdf?nodeid=619905&vernum=-2 [accessed July 2016]
- Anderson JG, Bodin P, Brune JN, Prince J, Singh SK, Quass R, Onate M, 1986. Strong Motion from the Michoacan, Mexico, Earthquake, Vol. 233. Science: p.1043-1049.
- Anderson JG, Lee Y, Zeng Y, Day S, 1996. Control of Strong Motion by the Upper 30 Meters, Bulletin of the Seismological Society of America, Vol. 86, No. 6: pp. 1749-1759.
- Brillon, C., 2016. North Coast Geohazards – 2016 Seismology Update; Geological Survey of Canada, Open File 8052, 14 p. doi:10.4095/298753 http://ftp.maps.canada.ca/pub/nrcan_rncan/publications/ess_sst/298/298753/of_8052.pdf [accessed July 2018]
- Brillon C, Cote MM, Hunter JA, 2015. HVSR analysis of preliminary Kitimat ambient noise survey, Geological Survey of Canada, Open File 7793; 7 pages, doi:10.4095/295976 http://ftp.maps.canada.ca/pub/nrcan_rncan/publications/ess_sst/295/295976/of_7793.pdf [accessed July 2018]
- Clague, JJ, 1977. Surficial Geology, Kitimat, British Columbia, Geological Survey of Canada, Open File 470, doi:10.4095/129271 http://ftp.maps.canada.ca/pub/nrcan_rncan/publications/ess_sst/129/129271/of_0470.pdf [accessed July 2018]
- Clague, JJ, 1985. Deglaciation of the Prince Rupert-Kitimat area, British Columbia, Canadian Journal of Earth Sciences, Vol. 22; p. 256-265
- Conway KW, Barrie JV, 2018. Large bedrock slope failures in a British Columbia, Canada fjord: first documented submarine sackungen; Geo-Marine Letters, vol. 38 (3), p. 195-209.
- Crow HL, Hunter J, Brillon C, Brewer K, Cote M, Allen T, Cassidy J, 2015a. Soft soil response investigations in Kitimat, BC – some preliminary results; in proceedings of the 11th Canadian Conference on Earthquake Engineering, Victoria, BC, July 21-24, 2015

- Crow HL, Good RL, Hunter JA, Burns RA, Reman A, Russell HAJ, 2015b. Borehole geophysical logs in unconsolidated sediments across Canada, Geological Survey of Canada, Open File 7591; 39 pages, doi:10.4095/295753
http://ftp.maps.canada.ca/pub/nrcan_rncan/publications/ess_sst/295/295753/of_7591.zip [accessed July 2018]
- Dix, CH. 1955. Seismic Velocities from Surface Measurements, *Geophysics* 20, no. 1 (January 1955): 68–86.
- Dolmage, V. 1956. Geology of Kitimat Area British Columbia; Report prepared for the Township of Kitimat; 29p.
- Gartner Lee, 2002. Kitimat Landfill Investigation, Kitimat, BC, Project 22-731; Report prepared for the District of Kitimat.
- Golder, 2014. Appendix 17.11 – Dredgeate Disposal Site (DDS) Technical Assessment Report; Report prepared for Rio Tinto Alcan as part of the Terminal A Extension Project Environmental Assessment Certificate Application; 278 pages
https://a100.gov.bc.ca/appsdata/epic/documents/p414/d39051/1432583408865_XRhmvjnGQ0LHChxg6Z4Tlv7Qc5tpX0nY0VwQSnnPGNx2FNVYhQCr!-14610924!1432577862966.pdf [accessed July 2016]
- Gosselin, J. M. 2016. Seismic hazard site assessment in Kitimat, British Columbia, via Bernstein-polynomial-based inversion of surface-wave dispersion (MSc. Dissertation). University of Victoria School of Earth and Ocean Sciences, Victoria, BC, Canada
- Gosselin JM, Cassidy JF, Dosso SE, Brillon C, 2017. Probabilistic seismic hazard site assessment in Kitimat, British Columbia from Bayesian inversion of surface-wave dispersion; *Canadian Geotechnical Journal*, doi.org/10.1139/cgi-2017-0265
- Hunter JA (ed.), Crow HL (ed.), 2015. Shear wave velocity measurement guidelines for Canadian seismic site characterization in soil and rock, Earth Sciences Sector, General Information Product 110, 2015; 226 pages, doi:10.4095/297314
http://ftp.maps.canada.ca/pub/nrcan_rncan/publications/ess_sst/297/297314/gip_110_e.pdf [accessed July 2018]
- Hunter, J A M; Burns, R A; Good, R L; Pelletier, C F; A compilation of shear wave velocities and borehole geophysics logs in unconsolidated sediments of the Fraser River Delta, British Columbia; Geological Survey of Canada, Open File 3622 (ed.rev.), 2016. doi.org/10.4095/298718
http://ftp.maps.canada.ca/pub/nrcan_rncan/publications/ess_sst/298/298718/of_3622_rev.zip [accessed July 2018]
- Hunter, JA, Pullan SE, Burns RA, Good RL, Pugin A, Skvortsov A, Goriainov NN, 1998. Downhole seismic logging for high-resolution reflection surveying in unconsolidated overburden; *Geophysics*, Vol. 63, No. 4, p. 1371-1384

- Hunter, JA, Douma M, Burns RA, Good RL, Pullan SE, Harris JB, Luternauer JL, Best ME, 1998. Testing and application of near-surface geophysical techniques for earthquake hazards studies, Fraser River delta, British Columbia; *in* Geology and Natural Hazards of the Fraser River Delta, British Columbia, (ed.) JJ Clague, JL Luternauer, and DC Mosher; Geological Survey of Canada, Bulletin 525, p.123, 145
http://ftp.maps.canada.ca/pub/nrcan_rncan/publications/ess_sst/210/210031/bu_525.pdf [accessed July 2018]
- Hunter JA, Crow HL, Brooks GR, Pyne M, Motazedian D, Lamontagne M, Pugin AJ-M, Pullan SE, Cartwright T, Douma M, Burns RA, Good RL, Kaheshi-Banab K, Caron R, Kolaj M, Folahan I, Dixon L, Dion K, Duxbury A, Landriault A, Ter-Emmanuil V, Jones A, Plastow G, Muir D, 2010. Seismic Site Classification and Site Period Mapping in the Ottawa Area Using Geophysical Methods; Geological Survey of Canada, Open File 6273, 1 DVD.
http://ftp.maps.canada.ca/pub/nrcan_rncan/publications/ess_sst/286/286323/of_6273.zip [accessed July 2018]
- Ivanov, J. and Miller, R.D. 2004. Semi-automatic Picking of First Arrivals through Cross Correlation Using Spline Interpolation Applied to Near-Surface Seismic Surveys; in Proceedings, Symposium on the Application of Geophysics to Engineering and Environmental Problems SAGEEP 17, Colorado Springs, CO., p. 1420-1425
- Konno K, Omachi T, 1998. Ground motion characteristics estimated from spectral ratio between horizontal and vertical components of microtremor, Journal of the Seismological Society of America, Vol. 88, No. 1, February, pp. 228-241.
- Kramer SL, 1996. Geotechnical Earthquake Engineering. New Jersey: Prentice Hall, 653p.
- Martin GR, Dobry R, 1994. Earthquake Site Response and Seismic Code Provisions, NCEER Bulletin, Vol. 8: 121-129.
- Nakamura Y, 1989. A method for dynamic characteristics estimation of subsurface using microtremor on the ground surface, Quarterly Report of RTRI, vol. 30, No. 1, pp. 25 to 33
- Pugin A J-M, Pullan S, Hunter JA, 2013. Shear-wave high-resolution seismic reflection in Ottawa and Quebec City, Canada, The Leading Edge 32, 3(2013); pp. 250-255, doi:10.1190/tle32030250.1
- SESAME, 2004. Guidelines for the Implementation of the H/V Spectral Ratio Technique Using Ambient Noise Measurements, Processing, and Interpretation, SESAME European Research Project WP12, Deliverable D23.12.
- Shaw, J; Stacey, C; Wu, Y; Lintern, G; 2017. Anatomy of the Kitimat fiord system, British Columbia; Geomorphology, vol. 293, 2017 p. 108-129
- Stacey, C D; Lintern, D G; Enkin, R J; 2018. Multifaceted re-analysis of the enigmatic Kitimat slide complex; Sedimentary Geology, vol. 369, p. 46-59